Physics and Chemistry of the Earth 144 (2026) 104718

Contents lists available at ScienceDirect

Physics and Chemistry of the Earth

journal homepage: www.elsevier.com/locate/pce

Comprehensive characterization of natural fracture networks of the Zubair Formation in North Rumaila oilfield

Fadia W. Al-Halfi, Amna M. Handhal *, Hussein B. Ghalib

Department of Geology, College of Science, University of Basrah, Basrah, Iraq

ARTICLE INFO

Keywords:
Natural fractures
Borehole image logs
Zubair formation
North Rumaila oilfield
Secondary porosity
Reservoir characterization

ABSTRACT

The Zubair Formation serves as a crucial clastic sedimentary reservoir in southern Iraq, greatly contributing to hydrocarbon exploitation. Natural fractures affect fluid movement and reservoir efficiency, even though the reservoir is highly productive. This is the first multiscale characterization of fractures in the Zubair clastic reservoir. This study comprehensively analyzes natural fractures in the Zubair Formation using data from 15 wells. To classify fracture types, determine fracture orientations, and enable fracture diagnosis in non-imaging wells through log calibration, the methodology integrates core and thin-section samples, borehole image logs, and conventional well logs. Results showed that open fractures account for 44.25% of all natural fractures, and fracture permeability (Kf) varied from 52.75 to 303.84 Darcy, indicating a highly conductive fracture network. These fractures create channels within the upper shale and upper sand zones, enhancing oil flow and reservoir productivity. Fractures primarily extend from the northwest to the southeast, while their predominantly vertical to sub-vertical geometry favors horizontal hydraulic communication. Secondary porosity index (SPI) values exceeding 0.75 in many fractured intervals demonstrate that fracturing significantly contributes to secondary porosity and reservoir quality. Fractured intervals consistently exhibit increased gamma-ray values, decreased bulk density, increased neutron porosity and acoustic transmission time, and positive resistivity separation, enabling reliable fracture identification in wells without image logs. Integrating fracture characterization with dynamic reservoir data, stress analyses, and advanced fluid flow modeling will improve understanding of fracture-controlled reservoir behavior.

1. Introduction

Accurate reservoir characterization and improved development strategies rely on natural fracture characterization (Nelson, 2001). Natural fractures markedly influence fluid flow, permeability, and the efficiency of hydrocarbon recovery in petroleum reservoirs (Narr et al., 2006). The presence of fractures in low-permeability reservoirs facilitates fluid migration, whereas fractures in high-permeability reservoirs induce permeability anisotropy (Laubach et al., 2019). Traditional diagnostic techniques exhibit notable limitations despite their importance: core examination, while providing direct visual evidence, is constrained by limited area coverage, high cost, and partial recovery, especially within fractured intervals (Kulander et al., 1990; Lorenz and Cooper, 2017). Although thin-section petrography yields microscopic information on fracture-filling minerals and diagnostic relationships, it is restricted to small sample sets (Anders et al., 2014). Conventional well logs (density, gamma ray, resistivity, acoustic, and neutron) lack sufficient resolution to quantify specific fracture characteristics, though they can aid in identifying fractured zones by their characteristic responses (Tiab and Donaldson, 2015). Understanding fluid flow in fractured reservoirs requires the exact determination of fracture parameters including dip, azimuth, density, and aperture using image logs (such as FMI and UBI) (Luthi, 2001; Lai et al., 2018). However, to evaluate the petrophysical impact of fractures on reservoir parameters, image logs alone are insufficient (Aghli et al., 2020). Most wells are unable to provide imaging logs because of their high operational expenses and technical risks (Luthi, 2001). Fracture networks and their reservoir properties can be thoroughly described by combining a range of data types, such as thin sections (microns), cores (centimeters), image logs (meters), and traditional logs (tens of meters) (Gauthier et al., 2002; Wennberg et al., 2016).

Recent studies show that well logs and geophysical data are

* Corresponding author.
E-mail addresses: fadia.waleed@uobasrah.edu.iq (F.W. Al-Halfi), amna.handhal@uobasrah.edu.iq (A.M. Handhal), hussein.ghalib@uobasrah.edu.iq (H.B. Ghalib).

https://doi.org/10.1016/j.pce.2026.104718
Received 15 April 2026; Received in revised form 29 July 2026; Accepted 3 August 2026
Available online 5 August 2026
1474-7065/© 2026 Elsevier Ltd. All rights are reserved, including those for text and data mining, AI training, and similar technologies.

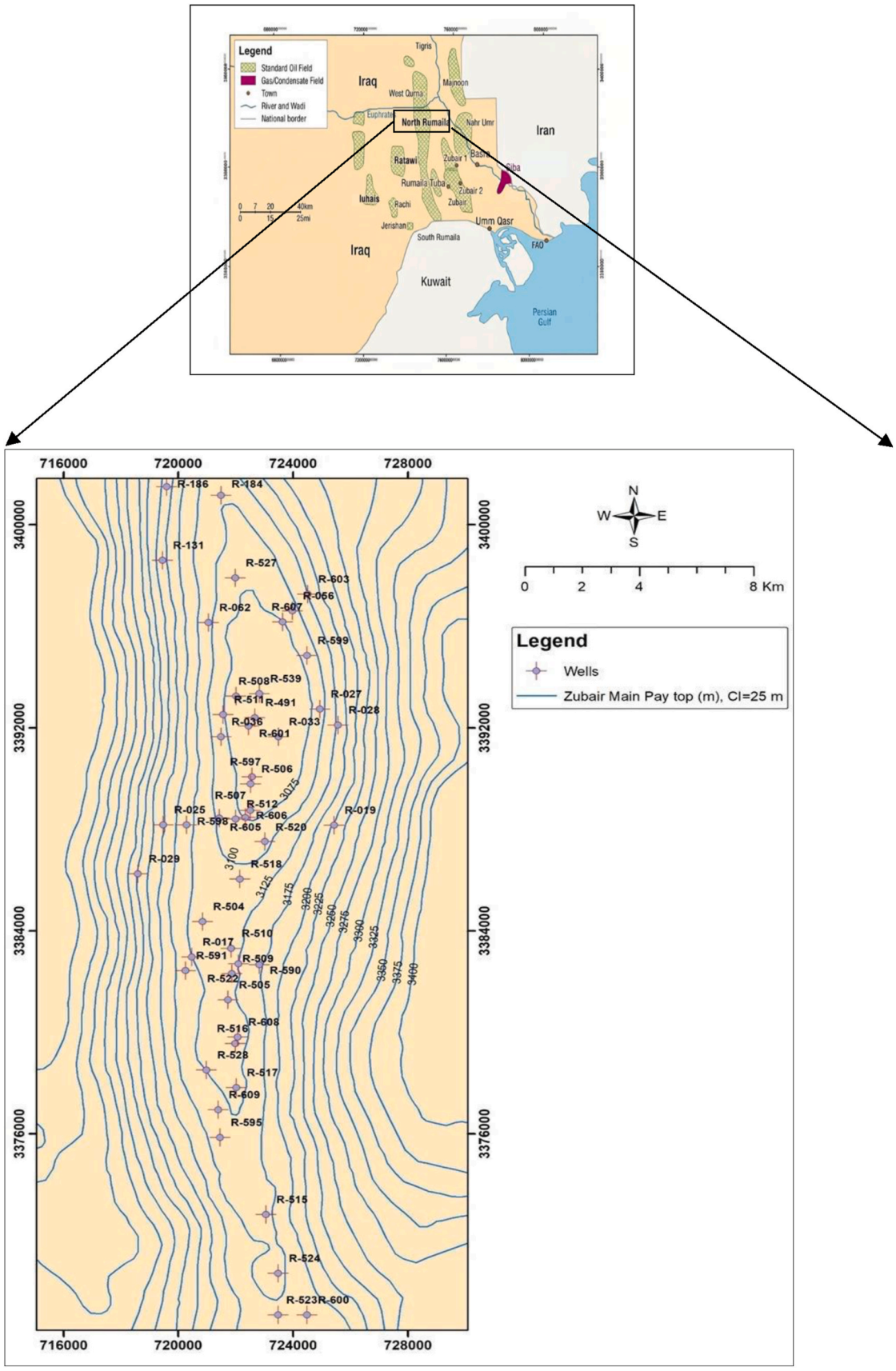


Fig. 1. Location map of the Zubair Formation, North Rumaila oilfield.

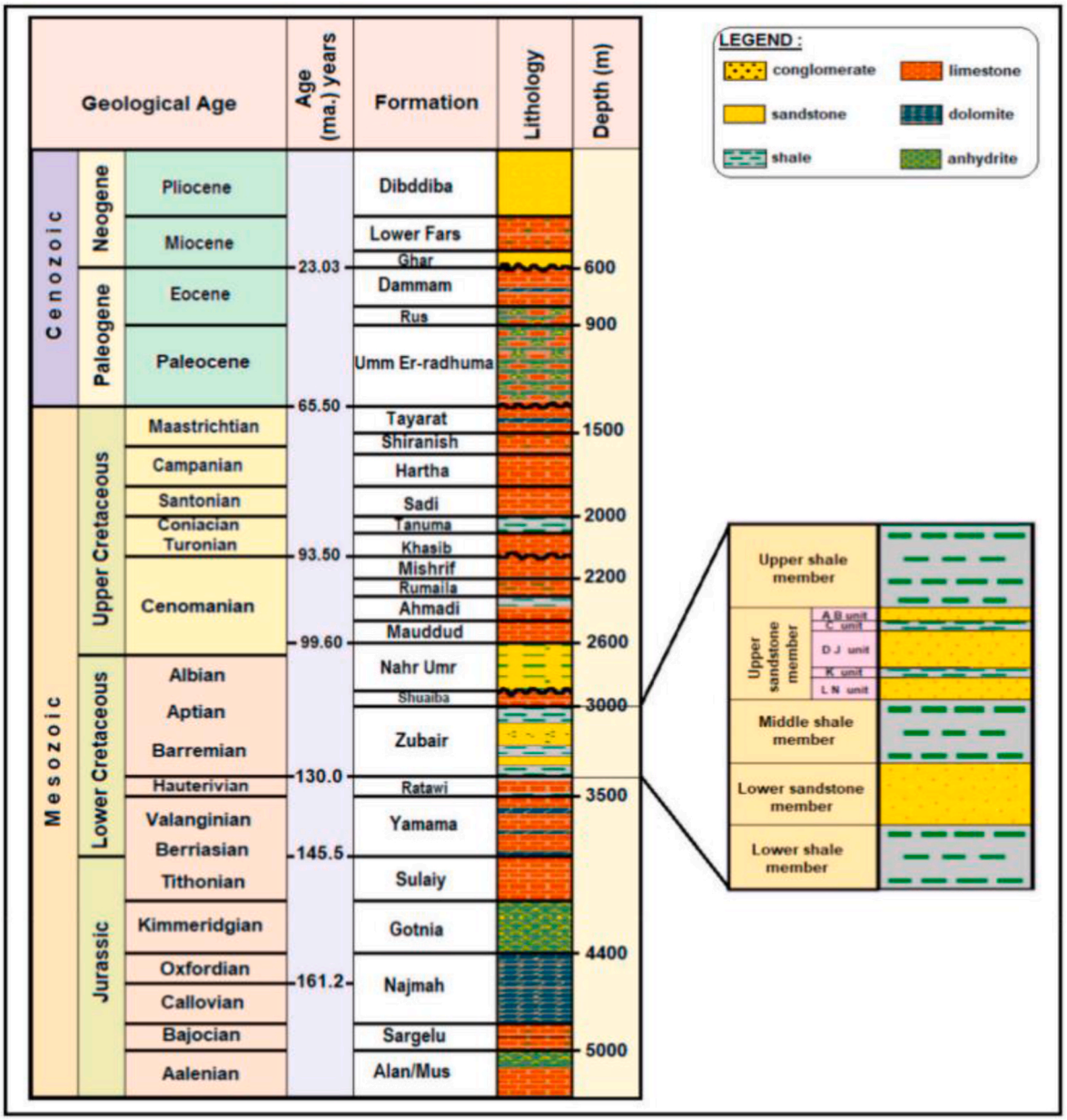


Fig. 2. Stratigraphic column of the Rumaila Oilfield, southern Iraq (after Handhal et al. (2019)).

Table 1
Summary of studied well data (available: ✓; missing: ×).

Well Name	Conventional Logs	FMI Logs	Cores	Thin Sections
R-520	✓	✓	×	×
R-523	✓	✓	×	×
R-516	✓	✓	×	×
R-527	✓	✓	×	×
R-598	✓	✓	×	×
R-491	✓	✓	×	×
R-518	✓	✓	×	×
R-504	✓	×	×	×
R-505	✓	×	×	×
R-506	✓	×	×	×
R-507	✓	×	✓	✓
R-509	✓	×	✓	✓
R-511	✓	×	✓	✓
R-510	✓	×	✓	✓
R-512	✓	×	✓	✓

beneficial for comprehensive reservoir assessment, beyond fracture characterization. By integrating petrophysical, elastic, and geomechanical parameters from well-log data, Leisi et al. (2026) and Aftab et al. (2023) produced comprehensive reservoir quality indicators. Meanwhile, Leisi and Shad Manaman (2025a, 2025b) refined the geomechanical characteristics of structurally complex Iranian carbonate reservoirs using well logs and simultaneous seismic inversion. Additionally, Leisi et al. (2025) used geostatistical modeling and neural networks to predict elastic properties using only conventional log data. Although they emphasize reservoir quality and geomechanical characterization rather than directly addressing fracture networks, these studies illustrate a broader methodological trend: using complementary, multiple data sources to address the limitations of individual measurement types. The purpose of this study is to characterize natural fractures using a multi-source integrated approach combining core data, thin sections, image logs, and conventional logs.

The Zubair Formation is one of the most significant clastic hydrocarbon reservoirs in southern Iraq, contributing substantially to national

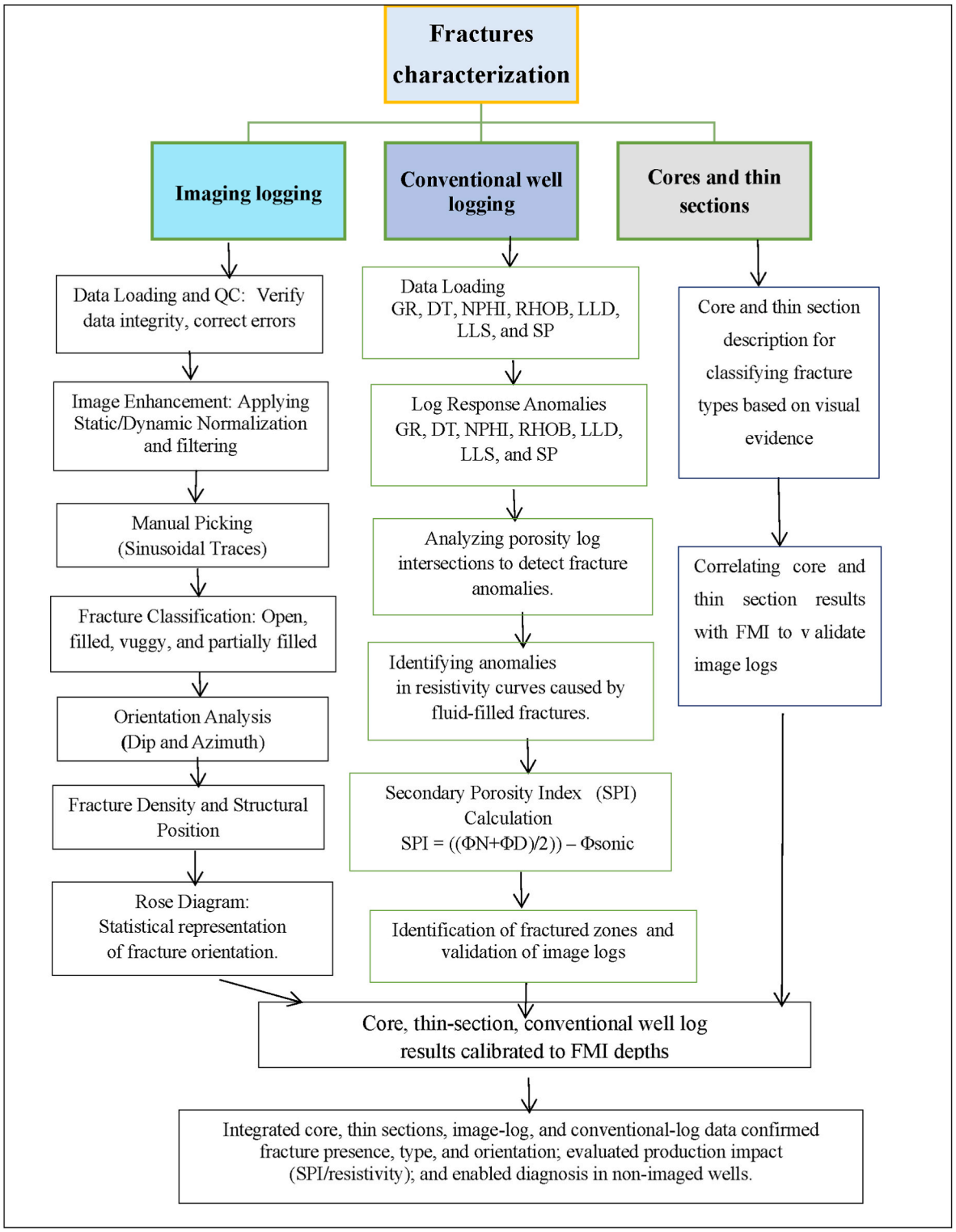


Fig. 3. An integrated methodology workflow for fracture characterization that illustrates the data inputs and analytical steps required to accurately characterize fractures.

oil production and providing a cornerstone for the energy economy of the country (Handhal et al., 2022). Over several decades, its high-porosity and high-permeability intervals have been the primary targets of exploration and development, particularly in major oilfields like Rumaila, West Qurna, and Zubair. In spite of this economic importance, reservoir performance is not solely determined by matrix properties; natural fractures play a critical role in enhancing or restricting fluid flow. For this reason, a comprehensive understanding of the spatial distribution, orientation, and connectivity of these fractures is essential from a scientific perspective, as well as for optimizing production methods. Inadequate characterization of fracture networks can result in suboptimal reservoir management, such as low sweep efficiency, early water breakthrough, and unexpected production heterogeneity. To reduce uncertainty and maximize ultimate hydrocarbon

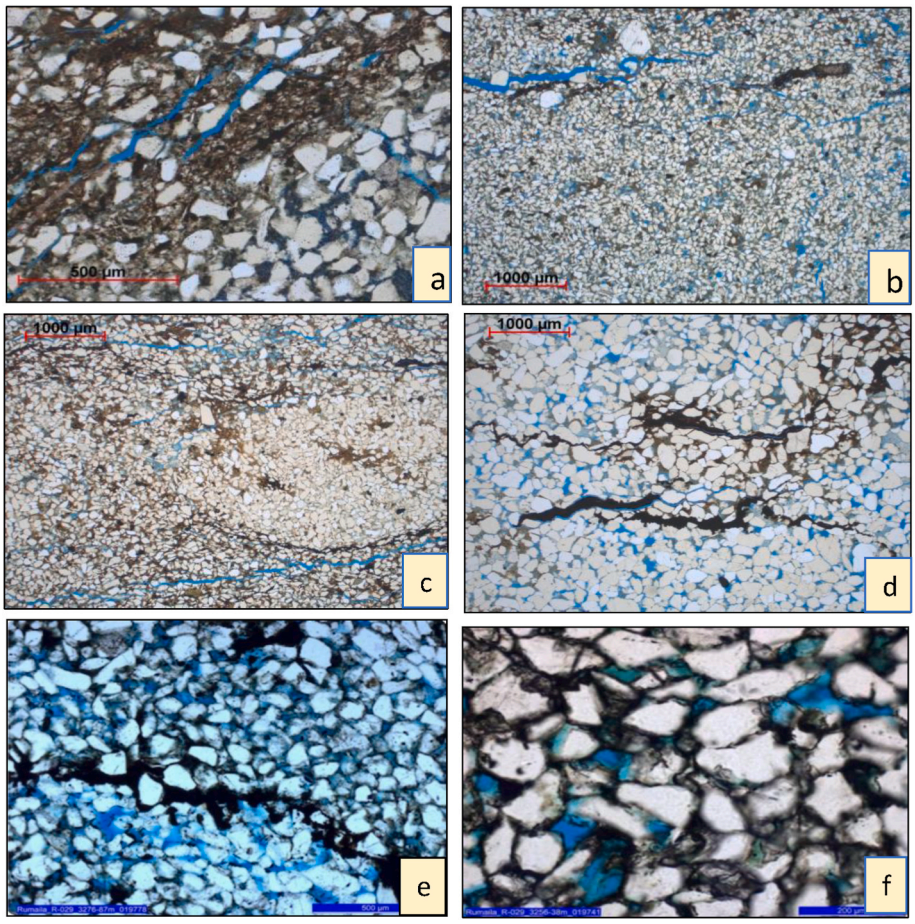


Fig. 4. Photographic of the Zubair Formation's natural fractures (a): open at 3296.25 m in well R-507, (b and c): partially filled at 3296.25 m in well R-509 and 3224.10 m in well R-511, (d and e): filled at 3268.53 m, and 3276.87 m in well R-510, and (f): vuggy at 3256.38 m in well R-512.

recovery from this strategically important formation, fracture characterization must be incorporated into reservoir models.

There has been significant development in fracture characterization techniques both globally and locally throughout the past decade. In the past few years, machine learning and deep learning have been used to automate fracture detection from conventional well logs, providing practical solutions when well image coverage is limited (Dong et al., 2022; Dong et al., 2024a; 2024b). In general, these efforts have focused on identifying fractures and classifying them according to their angle, rather than accurately classifying their type, determining their orientation, or linking them to reservoir productivity. In southern Iraq, borehole image logs have supported reservoir characterization in the Mishrif Carbonate Reservoir, the Buzurgan oilfield (Al-Ismaily, 2017), and structural analysis of the North Rumaila oilfield (Jaffar, 2018). Right up to today, only the Dammam Formation has been used for the interpretation of image logs about fractures in the Rumaila oilfield; no complete, multi-source dataset has been used (Shehab et al., 2023). The carbonate Mishrif Formation in the same oilfield has recently undergone a similarly comprehensive characterization using several types of sources, including core, thin-section, borehole imaging, and logging data (Al-Mohsen and Handhal, 2025). There is, however, a great deal of mechanical difference between clastic and carbonate lithologies, in addition to variation in fracture-porosity interactions within fracture systems. For a clastic reservoir like the Zubair Formation, no study has yet combined core observations, thin-section investigations, borehole image logs, and conventional well logs into a single, precise, and trustworthy technique, despite the increasing number of studies on fracture systems in carbonate reservoirs. Using precise orientation, structural location, quantitative reservoir quality indices, and detailed fracture classification, the current study aims to close this gap by offering the first comprehensive multi-scale characterization of fractures in the Zubair Formation.

In this integrated approach, six primary objectives are targeted: (i) developing a fracture classification system for the Zubair Formation; (ii) mapping fracture orientation using high-resolution borehole images; (iii) determining fracture distribution using high-resolution borehole images; (iv) evaluating fracture impact on reservoir quality through resistivity and Secondary Porosity Index analysis; (v) developing diagnostic criteria for fracture detection in wells without image logs by calibrating conventional log responses with fracture zones confirmed by image logs; and (vi) proposing a fracture characterization workflow that could be applied to similar clastic reservoirs throughout the world.

2. Geological setting

The Rumaila oilfield situated in southern Iraq, about 50 km west of Basrah city and 30 km west of the Zubair oilfield, is one of the world's largest oil fields. It lies between latitudes 30°55′7"N and 31°12′14"N and longitudes 47°14′14"E and 47°26′14"E (Jaffar, 2018) (Fig. 1). The Basrah Petroleum Company discovered the field in 1953. Tectonically, the Mesopotamian Foredeep Basin is divided into three main structural blocks: the Tigris, Euphrates, and Zubair blocks. The Rumaila oilfield is situated within the Zubair Block, which forms part of the Unstable Shelf on the Arabian Plate (Jassim and Goff, 2006). This region has experienced complicated Permian tectonic evolution, including rifting and passive margin formation associated with the opening of the Neo-Tethys, followed by convergence with the development of foreland basin in the Alpine orogeny (Buday, 1980; Aqrawi et al., 2010). The

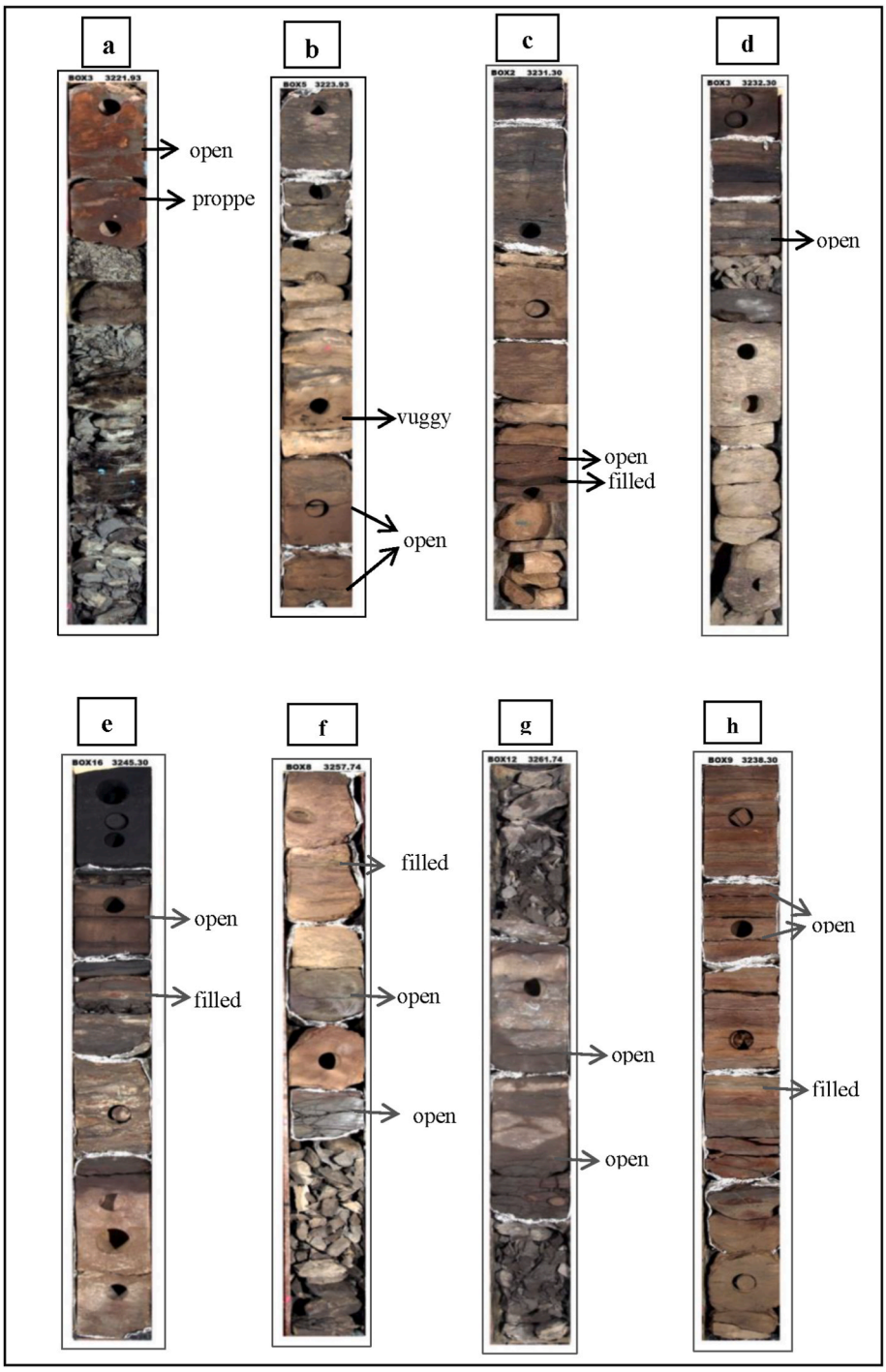


Fig. 5. The core photograph shows fracture classification in the Zubair Formation (a): mixed open and propped fractures at depth 3221.93-3222.93 m in well R-507; (b): mixed open and vuggy fractures at depth 3223.93-3224.93 m in well R-507; (c): mixed open and filled fractures at depth 3231.30-3232.30 m in well R-507; (d): open fractures at depth 3232.30-3233.30 m in well R-509; (e): mixed open and filled fractures at depth 3245.30-3246.30 m in well R-509; (f): mixed open and filled fractures at depth 3257.74-3258.74 m in well R-509; (g): open fractures at depth 3261.74-3262.74 m in well R-511; and (h): mixed open and filled fractures at depth 3238.30-3239.30 m in well R-511.

structure shows Zagros-related compression that began in the Middle Cretaceous and ended in the Miocene-Pliocene (Abdulnaby, 2019). Thus, the Mesopotamian Foredeep is an area of active subsidence with folding, fault reactivation, and diapirism. It contains such features as the Takadid-Qurna and Al-Batin fault systems trending NE-SW. The Rumaila oilfield is located as a structural element in the Zubair fault block in the Mesopotamian basin, this basin contains transverse fault systems developed during Precambrian periods. Fields in the vicinity formed above salt-filled, north-south-oriented Infracambrian rift basins. As a result of a collision between the Arabian and Eurasian plates during the Tertiary, these basins were remobilized (Jassim and Goff, 2006; Fouad, 2010; Fouad and Sissakian, 2011). Therefore, the Rumaila structure consists of a double-dipped, N-S trending anticline covering approximately 1600 km^2 with dimensions of 80 km by 20 km (Jaffar, 2018). The structure of the Rumaila oilfield is composed of two main segments, North Rumaila and South Rumaila, which are separated by a structural

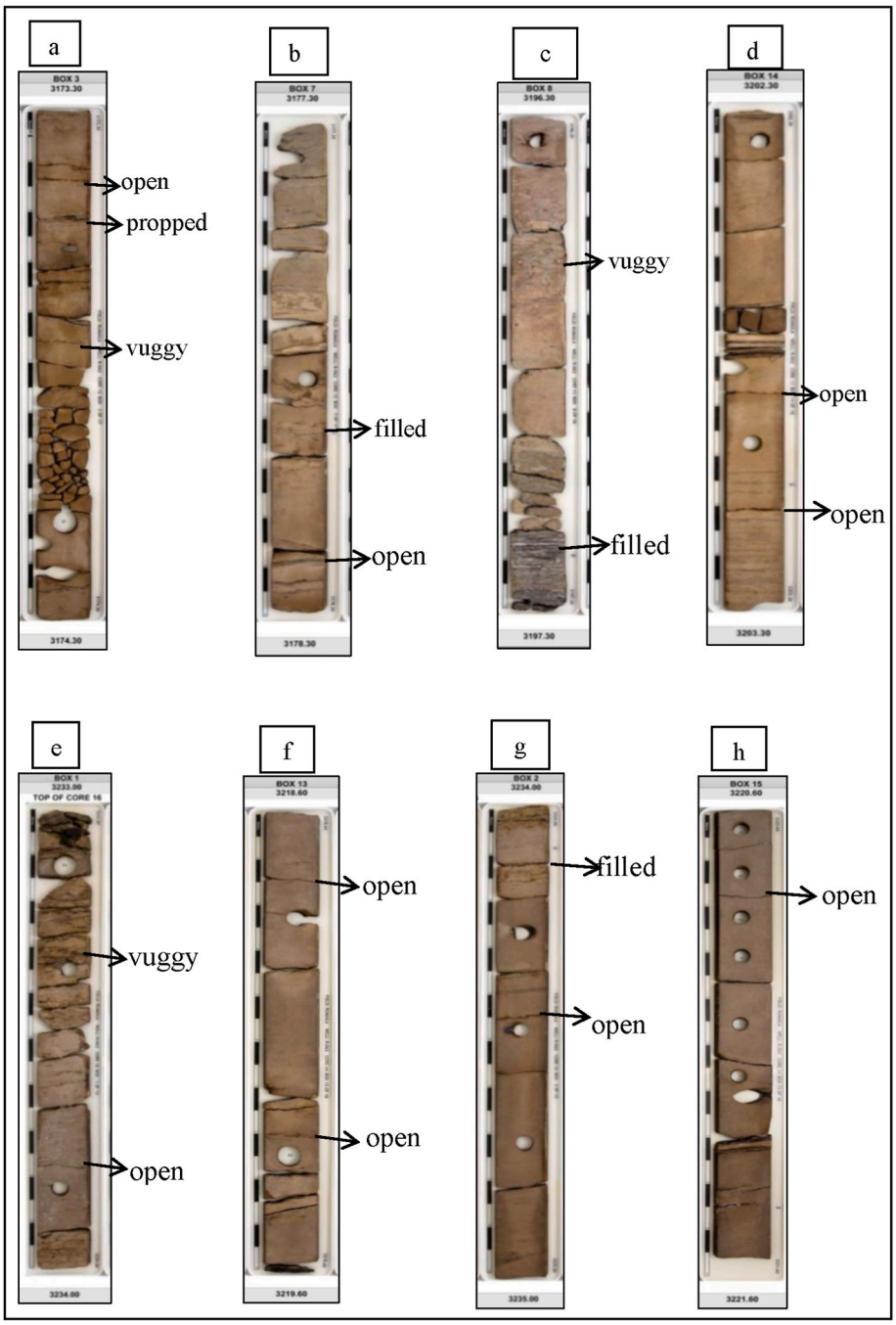


Fig. 6. The core photograph shows fracture classification in the Zubair Formation (a): mixed open, propped, and vuggy fractures at depth 3173.30-3174.30 m in well R-510; (b): mixed open and filled fractures at depth 3177.30-3178.30 m in well R-510; (c):mixed filled and vuggy fractures at depth 3196.30-3197.30 m in well R-510; (d): open fractures at depth 3202.30-3203.30 m in well R-510; (e): mixed open and vuggy fractures at depth 3233-3234 m in well R-512; (f): open fractures at depth 3218.60-3219.60 m in well R-512; (g): open and filled fractures at depth 3234.60-3235.60 m in well R-512; (h): open fractures at depth 3220.60-3221.60 m in well R-512.

saddle. The overall geometry is characterized by gentle flank dips of approximately 3° on the western side and 4° on the eastern side. This variation in dip angles reflects a slight structural asymmetry across the field, indicating differential tectonic influences during its development (Al-Ansari, 1993). Fractures caused by folds typically vary with the structure's position and curvature, which has significant implications for fracture formation (Hennings et al., 2000).

The Rumaila oilfield's structural framework controls its stratigraphic architecture, which includes cyclic carbonate, clastic, and evaporitic rocks with ages ranging from Late Jurassic to Recent (Jaffar, 2018). As the most important hydrocarbon system in this geologic column, the Early Cretaceous–Miocene petroleum system occupies a very important position. The Yamama and Zubair Formations are reservoir rocks, the Shranish, Tanuma, and Rus Formations are sealing rocks, and the Sulaiy and Yamama Formations are source rocks (Fig. 2). In the Lower Cretaceous succession on the Arabian Plate, the Zubair Formation (Hauterivian-Early Aptian) is one of the most significant siliciclastic depositional cycles (Bellen et al., 1959; Shafiei et al., 2018). It is made up of alternating sandstones, siltstones, and shale units that developed in fluvio-deltaic to shallow marine environments (Owen and Nasr, 1958; Al-Ameri and Zumberge, 2012). Mohammed et al. (2010) reported that sandstone constitutes 40–65% of the section in the study area. The

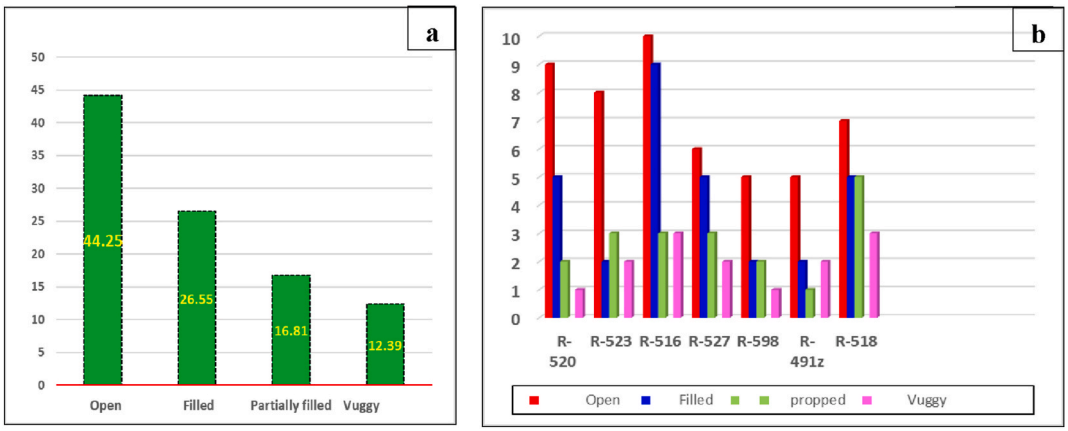


Fig. 7. Fracture density distribution by reservoir unit and well (a): Open fracture density for all wells (b): Percentages of fracture types for each well.

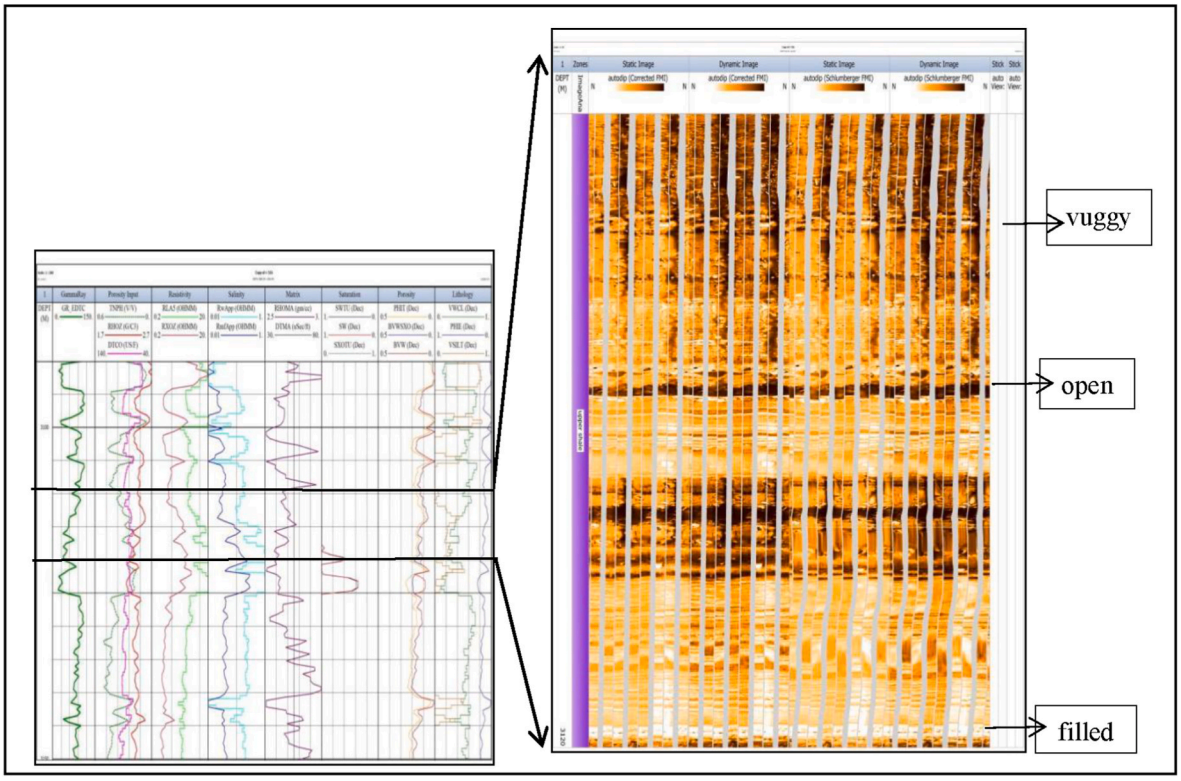


Fig. 8. Integrated Reservoir Characterization and Petrophysical Evaluation (GR, RHOB, NPHI, DT, LLD, LLS) and Image Log (FMI) for Well R-516, upper shale unit within depth range 3110-3120 m.

thickness of the Zubair Formation varies between 160 and 360 m in the study wells, with an average of 245 m. There are several depositional facies and diagenetic changes that influence the reservoir characteristics in the Zubair Formation (Saleh, 2019). A reservoir facies with levels of porosity of 12-24% and permeabilities of 10-1600 mD is optimal (Al-Aradi et al., 2022). There are five members of the Zubair Formation based on lithological differences (Fig. 2; Wells et al., 2017). These consist of the lower shale (Z/6), lower sand (Z/5), middle shale (Z/4), upper sand (Z/2A), and upper shale members, from oldest to youngest. The Upper Sand Member has five major units, which are referred to as the "main pay" because of their superior reservoir qualities. These consist of two shale units (C and K) and three sandstone reservoir units (AB, DJ, and LN) which act as barriers to vertical flow from base to top (Mohammed et al., 2010). A thin silt or shale lens is present during the formation of the AB unit, the lowest of these sandstone units. In the top sandstone section, the DJ unit is approximately 46–66 m thick, which is the primary reservoir interval. Due to its superior reservoir qualities, this sandstone unit, which is bounded by two siltstone strata, is the most productive interval. A reduction in thickness is observed toward the southern, western, and southwestern portions of the structure, whereas thickness progressively increases toward the east and north. A layer of sandstone interbedded with shale, siltstone, and shaly sandstone is considered as part of the LN unit. The increasing concentration of siltstone and shale near the base of the unit reflects a gradational transition into the underlying middle shale member and a progressive deepening of the depositional environment. There is a greater concentration of sand on the western flank of the LN unit than on its eastern side (Owen and Nasr, 1958. The Zubair Formation is underlain by the Ratawi Formation (interbedded limestones and shales) and overlain by the Shuaiba Formation (limestones and dolomites).

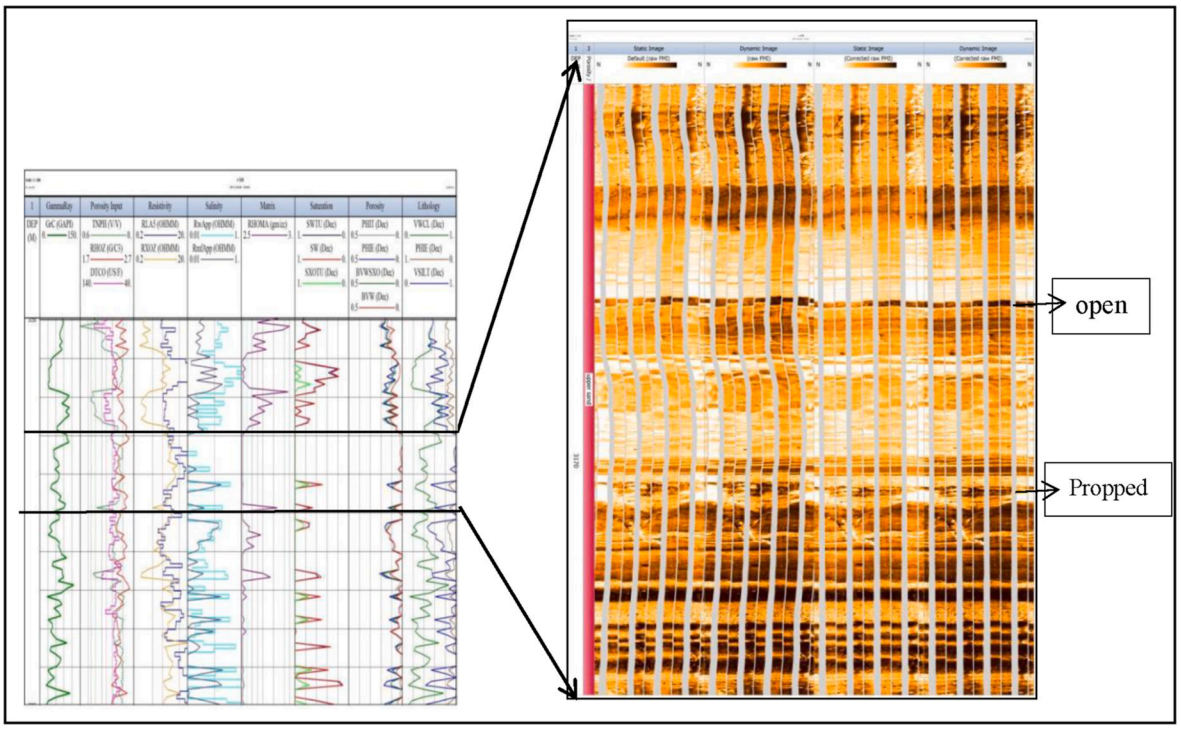


Fig. 9. Integrated Reservoir Characterization and Petrophysical Evaluation (GR, RHOB, NPHI, DT, LLD, LLS) and Image Log (FMI) for Well R-518, upper sand unit within depth range 3164–3174 m.

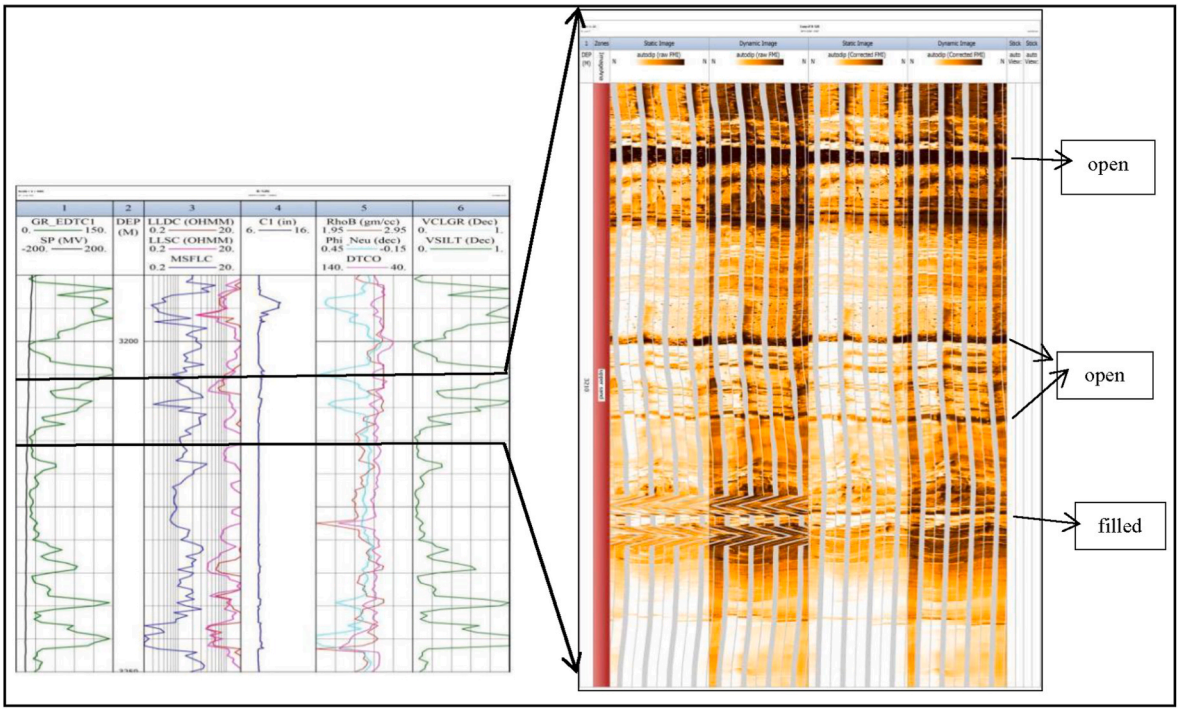


Fig. 10. Integrated Reservoir Characterization and Petrophysical Evaluation (GR, RHOB, NPHI, DT, LLD, LLS) and Image Log (FMI) for Well R-520, upper sand unit within depth range 3205–3215 m.

3. Dataset

Fifteen wells from the Zubair Formation in the North Rumaila oilfield were used to characterize natural fractures. The dataset includes conventional well logs from all fifteen wells: neutron porosity (NPHI), bulk density (RHOB), acoustic transit time (DT), gamma ray (GR), spontaneous potential (SP), shallow resistivity (LLS), and deep resistivity (LLD). High-resolution FMI logs were acquired from seven wells. Conventional cores were collected from five wells, and 100 thin sections were prepared from core intervals.

Table 1 displays the availability of conventional logs, FMI logs, core sections, and thin sections for 15 wells in this study.

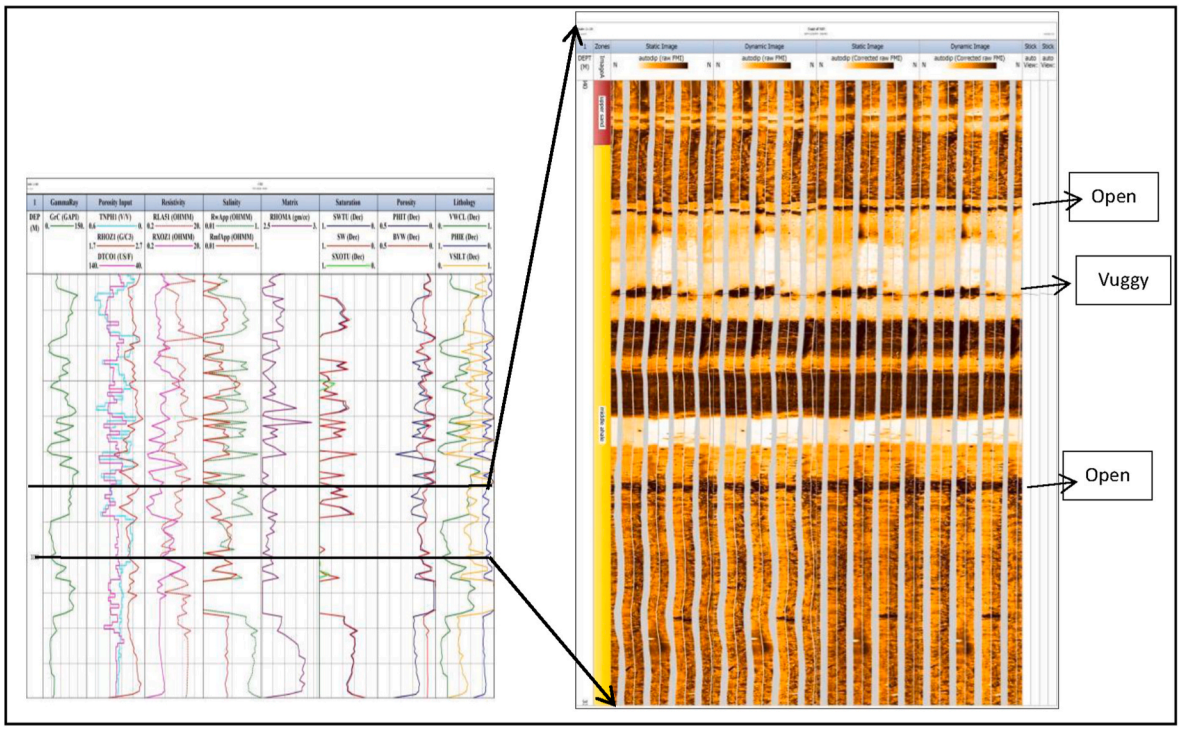


Fig. 11. Integrated Reservoir Characterization and Petrophysical Evaluation (GR, RHOB, NPHI, DT, LLD, LLS) and Image Log (FMI) for Well R-523, middle shale unit within depth range 3340–3350 m.

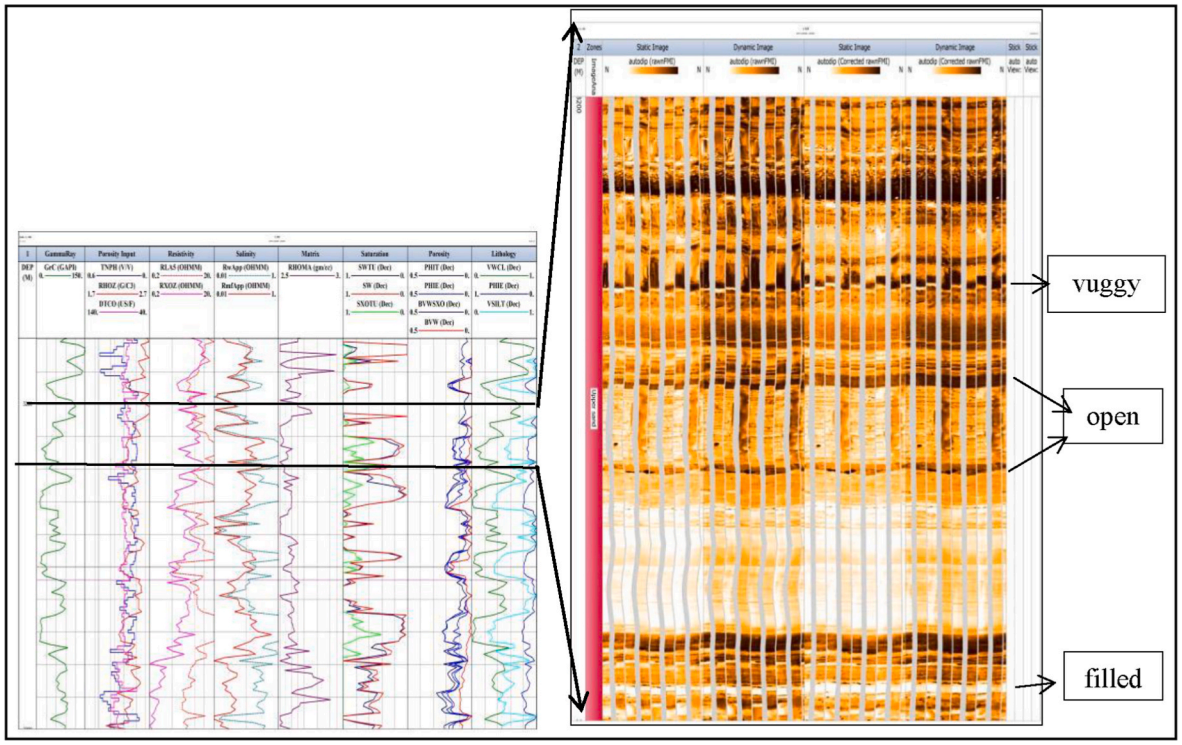


Fig. 12. Integrated Reservoir Characterization and Petrophysical Evaluation (GR, RHOB, NPHI, DT, LLD, LLS) and Image Log (FMI) for Well R-527, upper sand unit within depth range 3200–3210 m.

4. Materials and methods

4.1. Thin section petrography

Thin sections 30 μm thick were prepared from core samples according to standard procedures (Adams et al., 2017). The fracture characteristics were determined by microscopic examination. They were classified morphologically as open, filled, vuggy, or partially filled, and by origin as tectonic or diagenetic.

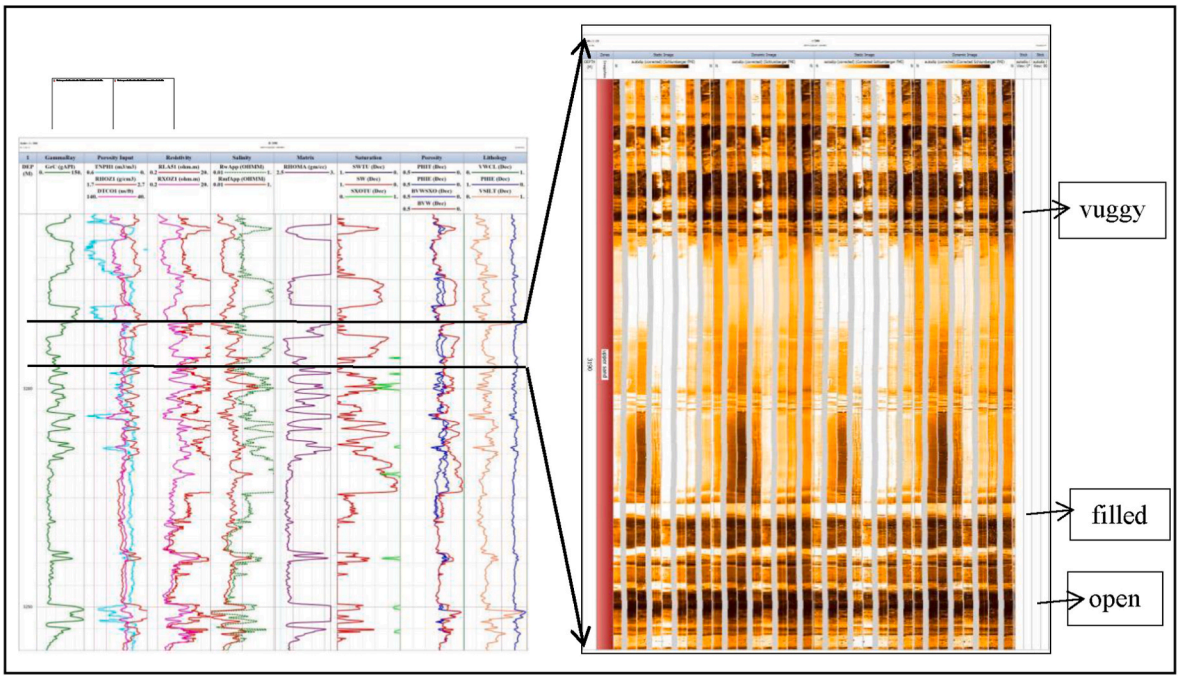


Fig. 13. Integrated Reservoir Characterization and Petrophysical Evaluation (GR, RHOB, NPHI, DT, LLD, LLS) and Image Log (FMI) for Well R-598, upper sand unit within depth range 3185–3195 m.

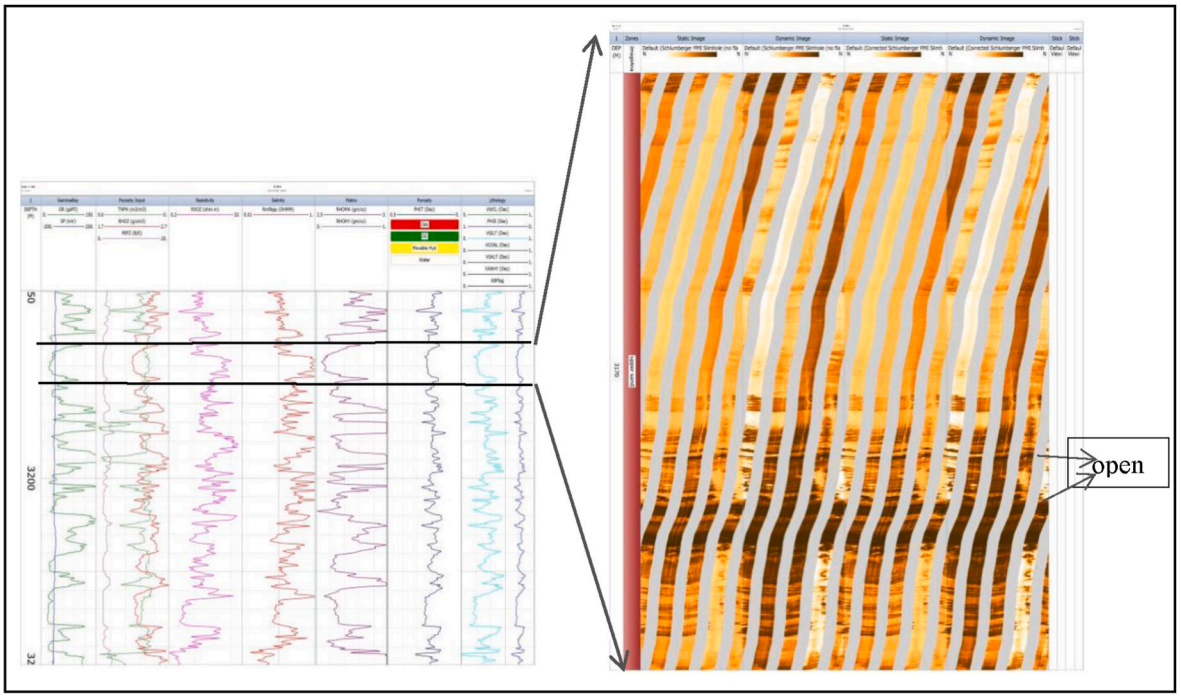


Fig. 14. Integrated Reservoir Characterization and Petrophysical Evaluation (GR, RHOB, NPHI, DT, LLD, LLS) and Image Log (FMI) for Well R-491, upper sand unit within depth range 3165–3175.

4.2. The core examination

Based on the total thickness of the formation in the selected wells, conventional core samples ranging in thickness from 150 to 245 m were examined and characterized to ensure a comprehensive representation of all reservoir zones as well as to accurately determine the vertical variations in natural fractures. The fractures were then classified according to:

1 Morphology: open, filled, vuggy, and partially filled
2. Orientation with respect to bedding: parallel to the bedding, inclined, or vertical.
3 Termination style: bedding-confined, fade-out/lensoid, or through-going

Core and thin sections observations were subsequently compared with image log data to verify orientation and ensure accurate

Table 2
Fractures density and structural position of study wells in the Zubair formation, North Rumaila oilfield.

Well	Fracture Density_ Frature per meter	Structural_Position
R-491	0.226	Fold crest (apex)
R-520	0.203	Fold crest (apex)
R-598	0.183	Fold crest (apex)
R-516	0.213	Fold crest (axial trend)
R-518	0.211	Fold crest (axial trend)
R-527	0.164	Fold plunge (northern nose)
R-523	0.163	Fold plunge (southern nose)
Field Average	0.195	

characterization.

4.3. Borehole image log analysis

4.3.1. Data quality control and preprocessing

FMI logs of selected wells were analyzed using Interactive Petrophysics (IP) version 4.5. The workflow includes the following steps:

1 The FMI logs were loaded in DLIS format and verified for completeness, accuracy, and depth.
2 Calibration of well depths: Wireline log analyses and drilling reports were used to match FMI log depths with reference well depths. This enabled accurate interpretation of reservoir characteristics and informed exploration and production decisions based on geological and petrophysical data that aligned with subsurface formations.
3 Data correction: Acceleration effects were removed, and button response was standardized using appropriate equations and wellbore stiffness adjustments. Accelerometer and magnetometer data were also used to correct instrument orientation.
4 Normalization of data and bias mitigation: The standardization of measurements reduced bias due to varying measurement ranges, improved data consistency, and increased the reliability of results. As a result of this standardization, log analysis becomes more accurate, allowing to identify true patterns and anomalies in the logs.

4.3.2. Feature identification and fracture classification

Sinusoidal curves representing planar features were picked either manually or automatically. Based on electrical response and mineral filling, four fracture types were distinguished:

1 Open fractures: Conductive (dark) continuous traces from drilling fluid invasion into open apertures. These tectonic-induced fractures are typically planar and vertically oriented (dip $> 75°$). Generally, aperture width and roughness influence permeability (Luthi, 2001; Nelson, 2001).
2 Closed fractures (healed): Resistive (bright) continuous fractures filled with calcite or anhydrite or possibly bitumen. Mineral fill reduces original porosity, creating fluid barriers (Nelson, 2001).
3 Partially filled fractures (propped): Discontinuous conductive traces with resistive segments. Fracture walls are still open, allowing fluid to flow through, even though minerals precipitate without sealing them completely (Luthi, 2001).
4 Vuggy fractures (solution-enlarged): Irregular, enlarged dark conductive features from dissolution along natural fractures. These significantly increase porosity and typically remain open during production (Aghli et al., 2020).

4.3.3. Fracture orientation analysis

A crucial factor in reservoir characterization is fracture orientation, which is determined by strike and dip angles (Narr et al., 2006). The dip azimuth of each detected fracture in the study area was determined following the classification of Zhao et al. (2025) which classified fractures based on dip angle into four groups: vertical (dip $> 75°$), high-angle (dip 45°-75°), low-angle (dip 15°-45°), and bedding-parallel (dip $< 15°$). Rose diagrams and histograms were generated from azimuth and dip data using IP software, which illustrates fracture orientation trends, bedding trends, and dip magnitude distributions.

4.3.4. Fracture density

The ratio of verified fracture picks from FMI image logs to the whole length of the logged interval is used in this study to define fracture density. This metric is always expressed as fractures per meter (fractures/m).

4.3.5. Fracture permeability calculation

Fracture permeability can be estimated using the parallel plate flow model, derived from Poiseuille's laws, which uses the simulation of fluid flow between two parallel plates as a geometric representation of the fracture opening (Erle, 2015; Tiab and Donaldson, 2015). FMI resistivity images were used to determine fracture aperture (wf), which relies on the additional conductivity caused by conductive drilling mud entering open fractures, as documented by Luthi and Souhaite (1990). For fracture permeability (Kf), this calculated aperture was used as an input parameter (wf) in the parallel plate flow model. The fracture permeability is expressed as:

$$\mathbf{kf} = \mathbf{8.444} \times \mathbf{10^6} \times \mathbf{wf^2}$$

where:

Kf: Fracture permeability in darcy
wf: The fracture width in cm

This relationship indicates that fracture permeability is highly sensitive to fracture aperture, increasing proportionally with the square of the aperture.

4.4. Conventional log analysis

Conventional logs (NPHI, RHOB, GR, DT, SP, LLS, and LLD) from fifteen wells were normalized and environmentally corrected (Ellis and Singer, 2007). The most important responses in fractured zones include:

Gamma Ray: Elevated values due to radioactive elements (Uranium and thorium) from fluid circulation (Rider, 1986; Nelson, 2001).

Spontaneous Potential: Deflections from fluid conductivity differences (Doll, 1949).

Density: Lower values from increased fracture porosity (Schlumberger, 1991).

Neutron: Altered responses from fluid movement and mineral leaching (Asquith et al., 2004).

Dual Laterolog-LLD: Increased separation indicating fracture-influenced invasion (Sibbit and Faivre, 1985).

The methodology also relies on calculating the secondary porosity index (SPI) to detect fractured intervals, SPI is calculated according to the equation (Schlumberger, 1991).

$$\mathbf{SPI} = \mathbf{ØND} - \mathbf{ØS}$$

$$\mathbf{ØND} = (\mathbf{ØN} + \mathbf{ØD})/\mathbf{2}$$

Where:

SPI: Secondary Porosity index
Ø ND: Neutron-Density porosity (total porosity)
Ø N: Neutron porosity
Ø D**:** Density porosity
Ø S: primary porosity (sonic), obtained from the acoustic transit time (DT) log

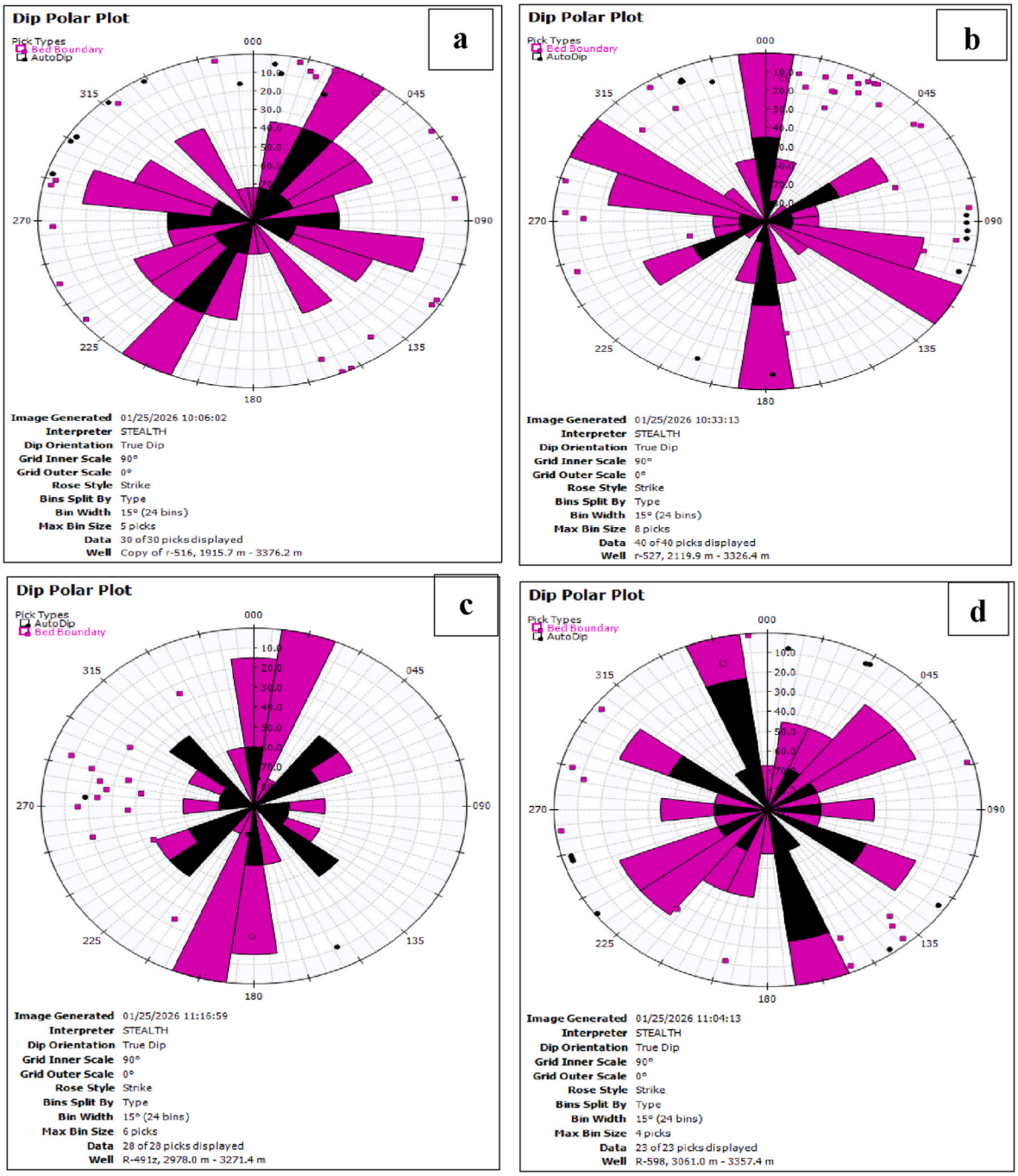


Fig. 15. Structural attitude of bed boundaries derived from image logs, featuring a stereonet to illustrate the formation dip and azimuth. (a): R-516, (b): R-527, (c): R-491, (d): R-598.

A significant increase in SPI is considered physical evidence of the presence of secondary voids resulting from fractures (Tiab and Donaldson, 2015).

Deep and shallow resistivity records were used to determine the geometric state of fractures. Open fractures are indicated by separation between curves resulting from the invasion of drilling mud filtrate into the fracture network. Conversely, curve overlays indicate closed or mineralized fractures, preventing fluid penetration (Asquith et al., 2004).

The flow chart below represents a comprehensive approach to characterizing fractures in the study area (Fig. 3).

5. Results

5.1. Core and thin section examination for fracture characterization

Core and thin-section analyses of the Zubair Formation reveal diverse fracture networks characterized by distinct genetic origins, spatial orientations, and morphology.

Fractures were classified as diagenetic or tectonic according to their origin. Fractures associated with tectonic activity are usually well-developed, planar, and extensible laterally, often cutting through the bedding planes and affecting diagnostic features. They result from regional stresses related to faulting, folding, and shearing the predominant stress regime during deformation is reflected in their consistent

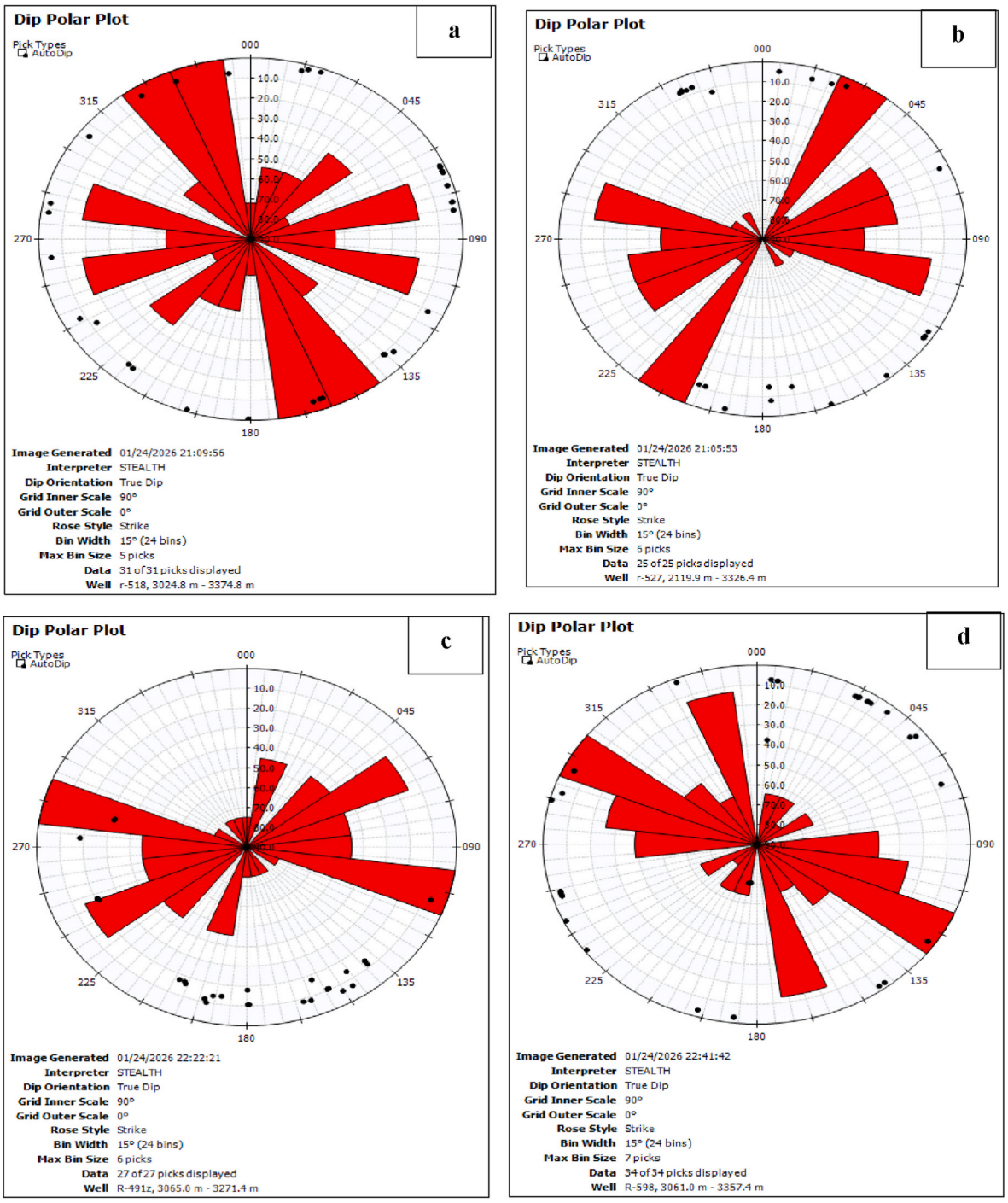


Fig. 16. Integrated orientation analysis of natural fractures obtained from image logs, featuring a rose diagram to illustrate the dominant strike trends. (a): R-518, (b): R-527, (c): R-491, (d): R-598.

orientation (Fig. 4a, b, and c).

In contrast, diagenetic fractures have an irregular morphology and are closely related to dissolution seams and stylolite. They are created by compaction, cementation, and mineral expansion after sediment deposition and lithification (Fig. 4d, e, and f).

According to core sample examinations, there is a widespread network of vertical and subvertical fractures intersecting the well wall in the study area, which would improve reservoir permeability significantly. Additionally, the examination revealed through-going fractures are more common than confined fractures. This is mechanical evidence that the formation has been under uniform tectonic stresses. This fracture network has contributed to the enhancement of vertical permeability of the reservoir (Cooke and Underwood, 2001; Laubach et al., 2009), (Figs. 5 and 6).

An examination of the morphology of core samples and thin sections revealed the following: open fractures are the most common type, where they exhibit visible apertures without mineral fill (Fig. 4a), (Fig. 5a, b, c, d, e, f, g, and h), (Fig. 6a, b, d, e, f, g, and h). Filled fractures, occluded by calcite and anhydrite, create localized barriers to fluid movement (Fig. 4d–and e), (Fig. 5c–e, f, and h), (Fig. 6b, c, and g). In contrast, partially filled fractures retain some connectivity through mineral-coated walls with residual open spaces (Fig. 4b–and c), (Fig. 5a),

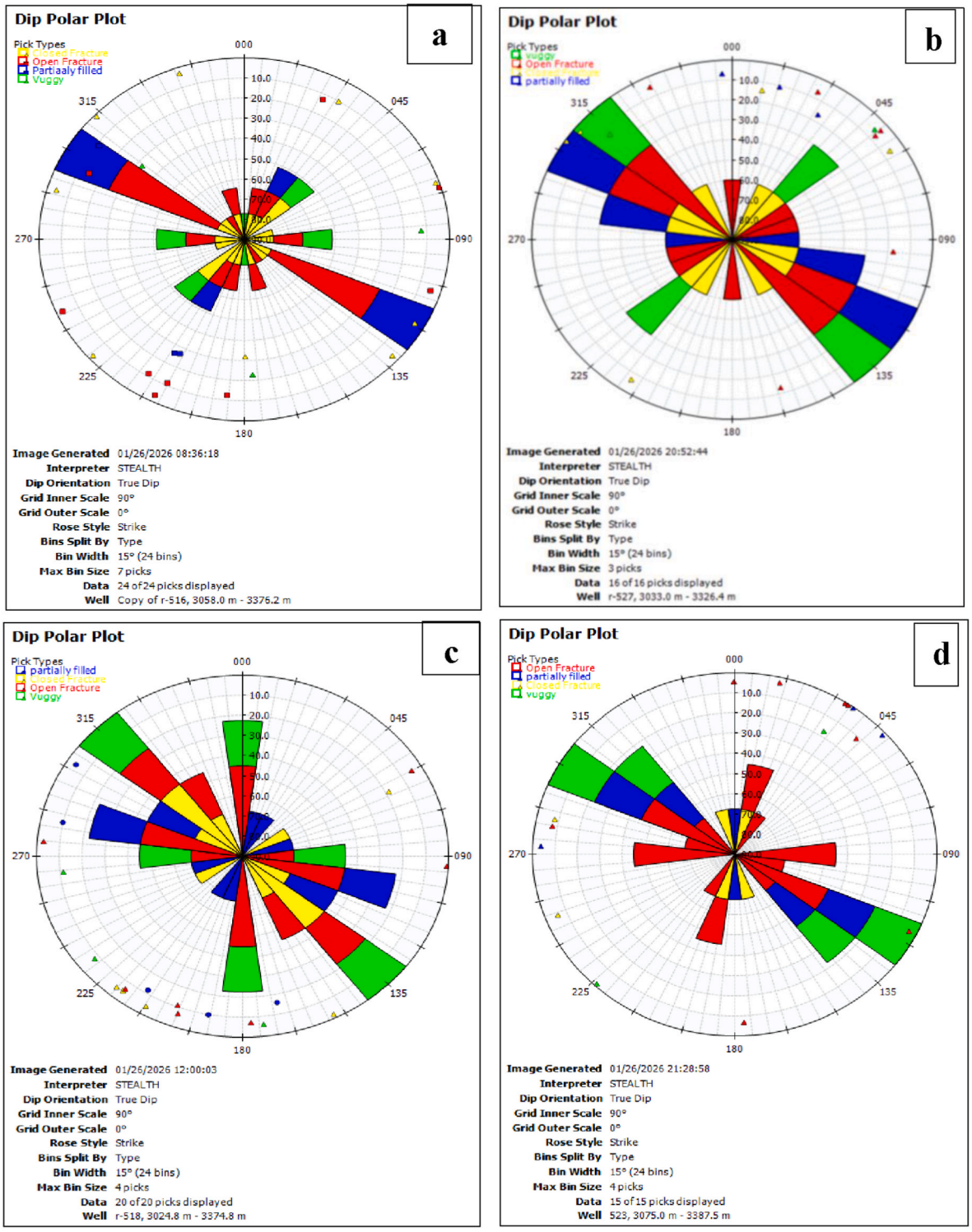


Fig. 17. Rose diagram shows us the type of fractures with its orientation a: (R-516), b: (R-527), c: (R-518), and d: (R-523), the colors Red (open fractures), green (vuggy fractures), blue (partially filled), yellow (filled fractures). (For interpretation of the references to color in this figure legend, the reader is referred to the Web version of this article.)

(Fig. 6a). Vuggy fractures, characterized by dissolution-enhanced porosity along fracture planes, significantly enhance storage capacity (Fig. 4f), (Fig. 5b), (Fig. 6a).

5.2. Image logs for fracture characterization

Natural fractures were identified in seven wells using image log analysis. Based on the electrical conductivity response and morphological features observed on FMI images, these fractures were classified into four types: open, partially filled, closed, and vuggy (Figs. 7–14). The high percentage of open fractures (44.25%) indicates a significant part of the natural fracture network is still conductive and able to support fluid movement. While partially filled fractures (16.81%) indicate intermediate stages of healing that might still have some residual

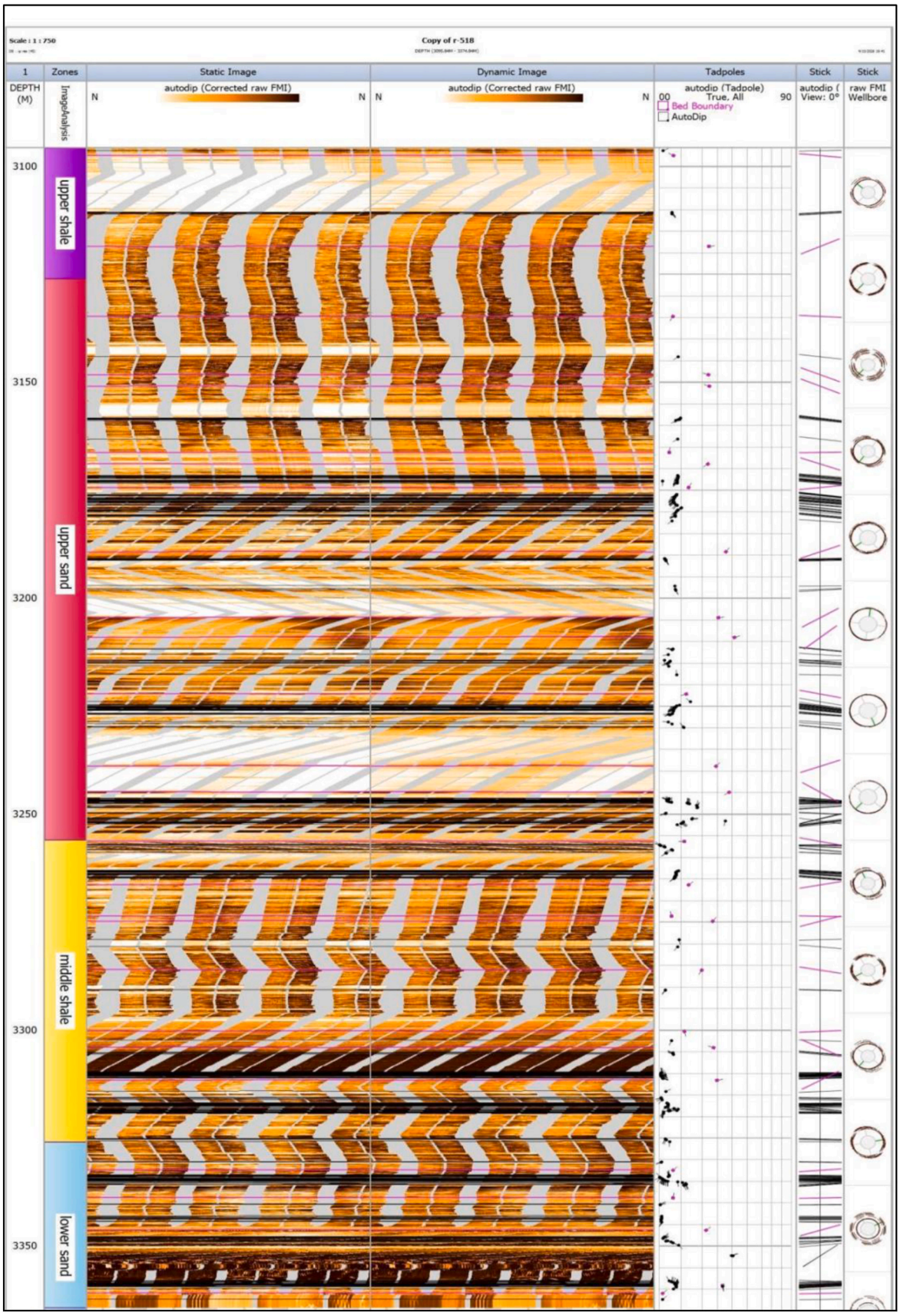


Fig. 18. Well R-518 orientation using Auto Dip calculation of fractures and bed boundary.

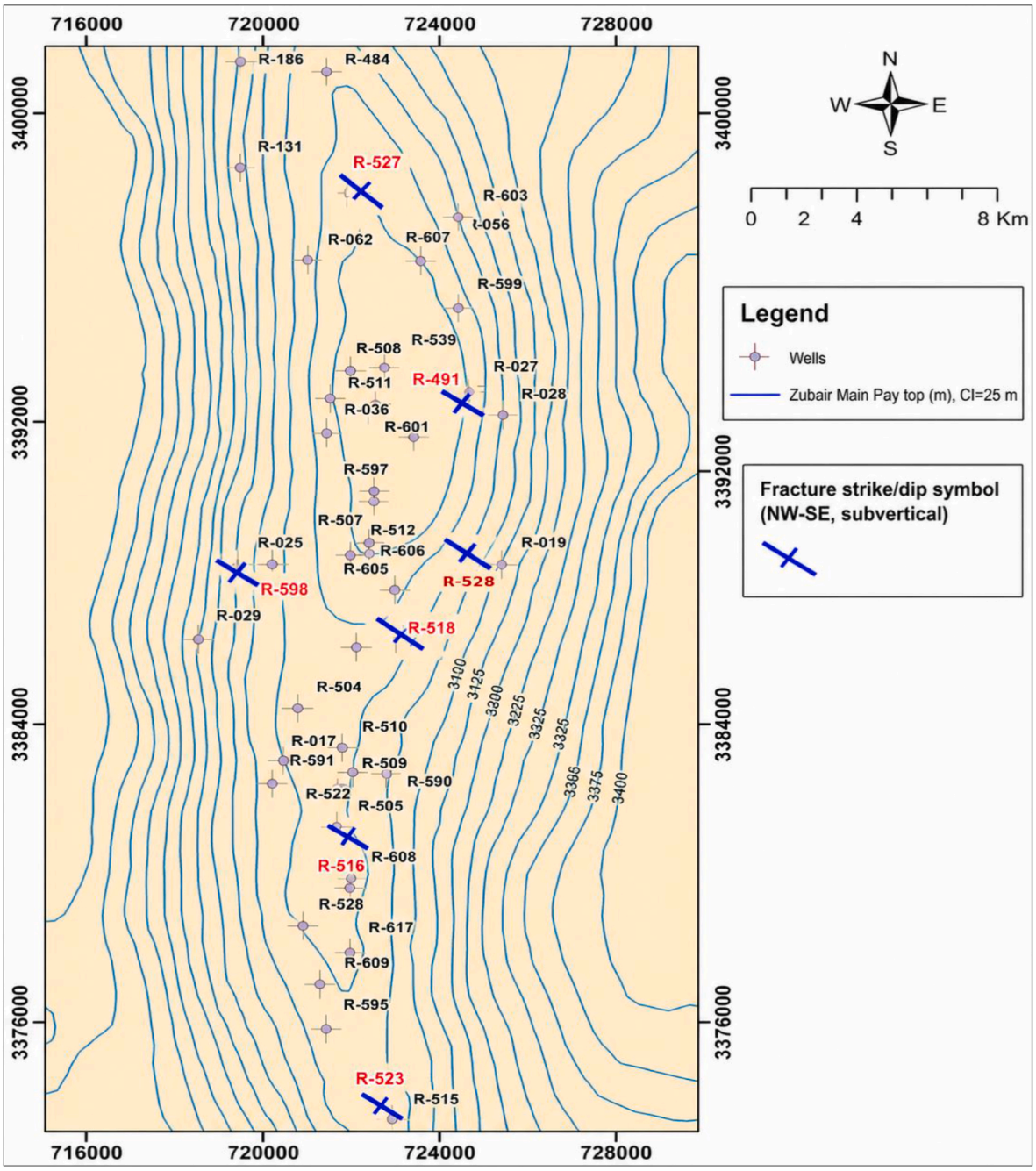


Fig. 19. The contour map of the Zubair Formation, North Rumaila oilfield, displays well positions alongside symbols indicating fracture strike and dip (NW-SE, subvertical), demonstrating the uniform regional fracture orientation throughout the study area.

Table 3
Summary of conventional log behavior by fracture type.

Fracture Type	GR	RHOB	NPHI	DT	ΔR	SPI
Open	Increase	Decrease	Increase	Increase	Positive	High
Partially Filled	Slight increase	Slight decrease	Slight increase	Slight increase	Weak	Low-Moderate
Closed	No change	No change	No change	No change	None	Minimal
Vuggy	Increase	Strong decrease	Strong increase	Increase	Strong	Highest

conductivity, closed fractures (26.55%) reveal post-fracturing mineralization. Although vuggy fractures are the least frequent type, accounting for only 12.39%, they are important due to their enhanced porosity resulting from dissolution along fracture planes. Integration of the thin-section petrography, core examinations, and image log data confirms that this classification is reliable across all scales and typical of the natural fracture population in the studied area, thus validating the fracture classification method.

The results showed that the wells located at the top of the structure (R-516, R-520, and R-491) recorded the highest density of open

Table 4
Fracture type and depth interval identification by analyzing anomalies observed on conventional well logs.

Well number	Depth) meter (	Fractures type	Well number	Depth) meter (	Fractures type
R-512	3027.4, 3059.5, 3125, 3302.3, 3245.6	Open	**R-504**	3072.9, 3077.9, 3133.9, 3339, 3152.4	Open
	3034, 3108, 3119	Filled		3217.4, 3349.9	Filled
	3078.7	Propped		3124.4	Vuggy
				3283.9, 3326.4	Propped
R-516	3114.7, 3116.2, 3140.7, 3166, 3358	Open	**R-505**	3088.4, 3100, 3115.5, 3173	Open
	3062.2, 3066.2, 3084.2, 3237.2	Filled		3309.2	Propped
	3075	Vuggy		3304, 3355	Vuggy
	3060.2	Propped			
R-518	3184.3, 3228.3, 3314.3	Open	**R-506**	3055.7, 3102.7, 3217.6, 3317.8	Open
	3256	Filled		3300	Filled
	3277.8	Propped		3032	Propped
	3340.3	Vuggy		3082	Vuggy
R-520	3209.5, 3235, 3133.5, 3152.8, 3071.5	Open	**R-507**	3029.8, 3191.8, 3256, 3093.8, 3371	Open
	3077.5, 3094.5, 3110.5, 3244	Filled		3328	Filled
	3049.5	Propped		3189.3	Propped
	3329, 3096.3, 3167.5	Vuggy			
R-523	3120.5, 3134.5, 3196, 3333	Open	**R-509**	3170.7, 3158, 3233	Open
	3145.5	Filled		3078, 3317.7	Filled
	3343, 3196.4	Propped		3286.4, 3237, 3415.9	Propped
	3250	Vuggy		3294.4	Vuggy
R-527	3174.9, 3314.9, 3210.9	Open	**R-510**	3116.9, 3275.5	Open
	3193.4	Filled		3077.3, 3172.2, 3247	Filled
	3061.9	Propped		3083	Propped
	3136.9, 3140.4	Vuggy			
R-598	3090.2, 3091.1	Open	**R-511**	3073.5, 3105.9, 3157.4	Open
	3265, 3280	Filled		3022.4, 3128	Filled
	3187	Vuggy		3232, 3239.6	Vuggy
				3244.4	Propped
R-491	3103, 3180.4	Open	**R-491**	3193.5	Propped
	3067, 3129.5	Filled		3063	Vuggy

fractures within the units (upper shale and upper sand) (Fig. 7a–and b), which is attributed to the concentration of tectonic tensile stresses at the maximum bending zone of the fold; these fractures act as super permeable pathways, which is consistent with the conclusions of Aguilera)1995) regarding the role of structural positioning in enhancing the fracture networks of clastic reservoirs.

5.2.1. *Density and structural position of the fractures*

Fracture densities for seven wells were derived from well imaging (FMI) data, revealing an average of 0.195 fractures per meter, with a range between 0.163 and 0.226 fractures per meter. Wells situated along the structure's crest axis (R-491, R-520, R-598, R-516, and R-518) consistently exhibited higher fracture densities, ranging from 0.183 to 0.226 fractures per meter, compared to those at the fold's plunging ends, as detailed in Table 2. Boreholes R-523 and R-527, positioned at the southern and northern plunging ends of the structure, respectively, recorded the lowest fracture densities, at 0.163 and 0.164 fractures per meter. As per fold-associated fracture models (Hennings et al., 2000), fracture densities are greater near the fold crest than at its plunging ends.

5.2.2. *Fracture orientation analysis*

Image logs from the study area revealed that the dips were mostly towards the east-northeast with gentle angles, suggesting the presence of bed boundaries rather than fractures. Fig. 15a, b, c and d illustrate that around 70% of AutoDip fracture selections are concentrated at steep angles exceeding 45°, while those associated with bed boundaries are mainly at lower angles. The Rose diagrams (Fig. 16a, b, c, and d) demonstrate a dominant NW-SE fracture orientation, accompanied by a secondary NE-SW orientation. In Fig. 17a, b, c, and d, rose diagrams with color codes were generated: red represents open fractures, blue indicates partially filled fractures, yellow signifies closed fractures, and green denotes vuggy fractures. The dip-angle distribution mentioned earlier was used in an auto-dip analysis, revealing that natural fractures intersect stratigraphic sequences through a wide network of orientations ranging from high-angle to sub-vertical (Fig. 18). The findings suggest that open fractures align in a northwest-southeast direction. This orthogonal fracture distribution, particularly of open fractures, points to tectonic influences stemming from stresses linked to the folding process in the structure's crestal area. This structural arrangement transforms the reservoir flow regime from a single-porosity system to a dual-porosity system, enhancing well productivity (Nelson, 2001).

5.2.3. *Fracture permeability*

In the wells under study, fracture permeability (Kf), which was determined using a parallel plate flow model based on aperture values derived from FMI, varied from 52.75 to 303.84 Darcy, with an average value of approximately 171.5 Darcy. Significant potential for improved directional permeability over fracture-dominated intervals, especially parallel to the predominant northwest-southeast direction, is suggested by this vast variance, which reflects variations in fracture aperture size, as demonstrated by the uniform NW-SE fracture strike shown in the studied wells (Fig. 19).

5.3. *Conventional log responses in fractured zones*

When image log data is combined with conventional well logs, the Zubair Formation shows comparable petrophysical responses at fractured intervals. These responses ensure that it is possible to identify fractured zones and classify different types of fractures based on distinctive log signatures in wells that lack image logs.

5.3.1. *Behavior of conventional logs in fracture zones*

In Table 3, the idealized petrophysical response (general trend) of conventional logs to different fracture types is summarized here, providing a framework for interpreting geophysical anomalies found in

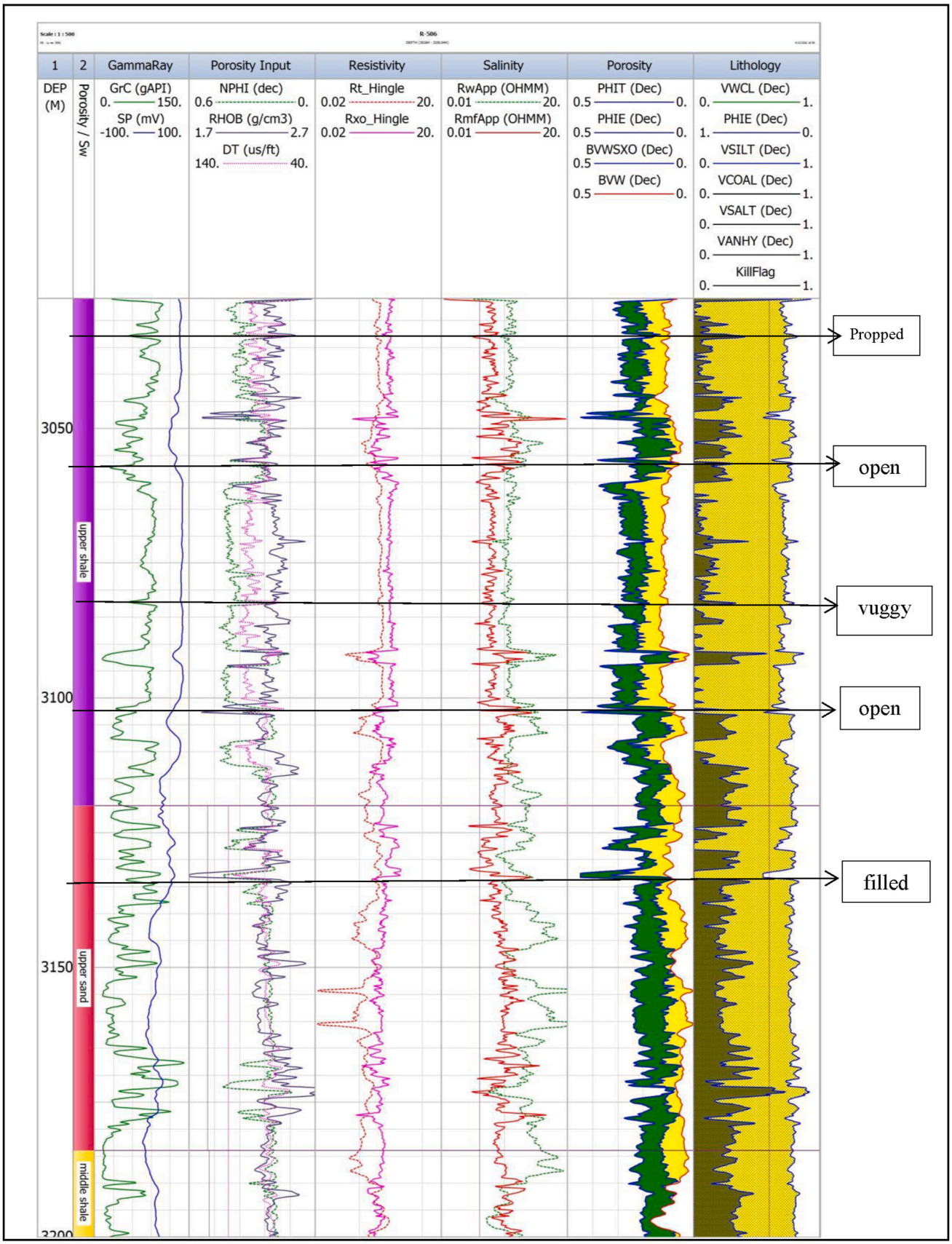


Fig. 20. Characterization of conventional log responses to natural fractures: open, filled, propped, and vuggy types.

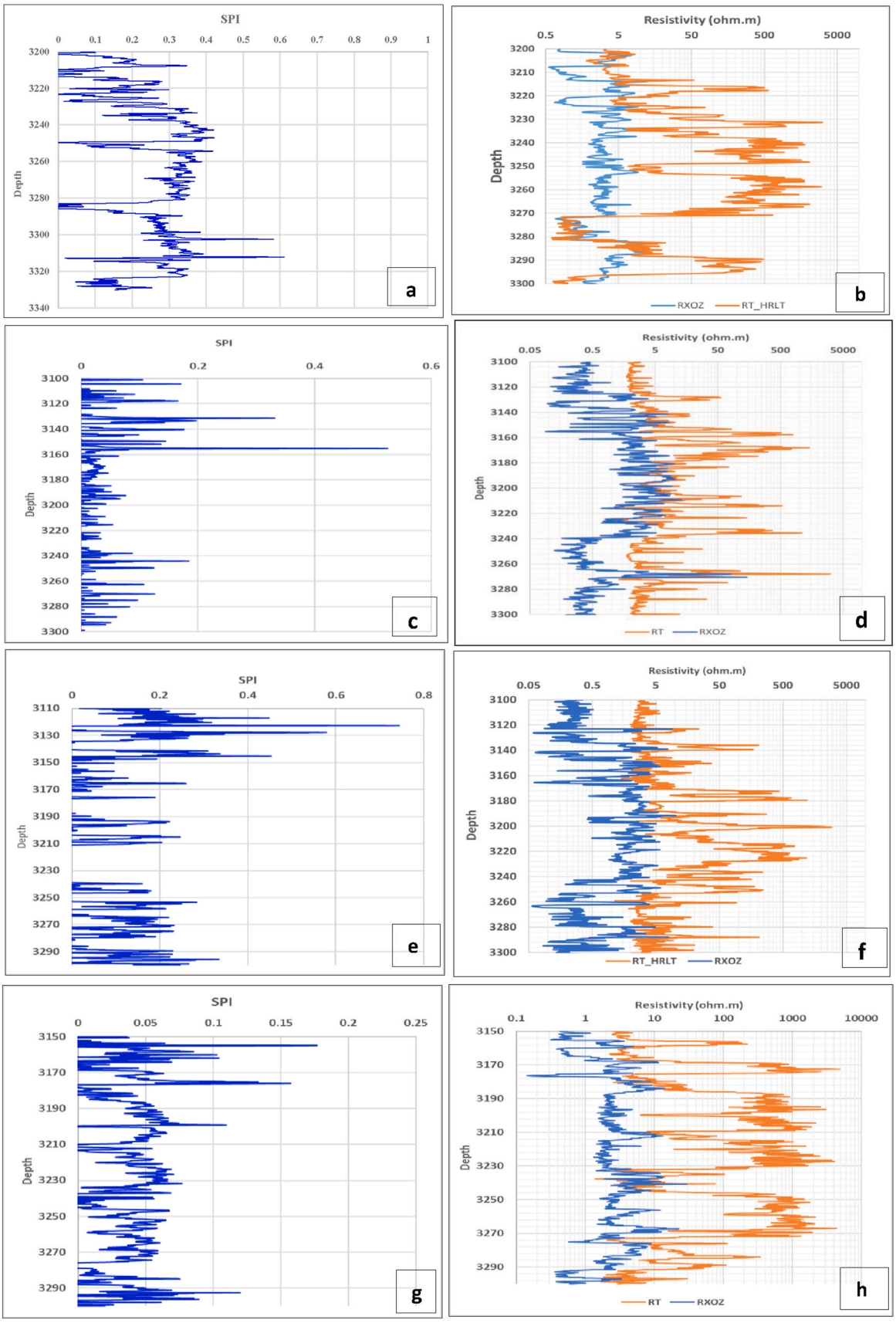


Fig. 21. Secondary porosity Index (SPI), Resistivity log separation indicating high permeable zone, (a and b): R-523, (c and d): R-527, (e and f): R-520, (g and h): R-516.

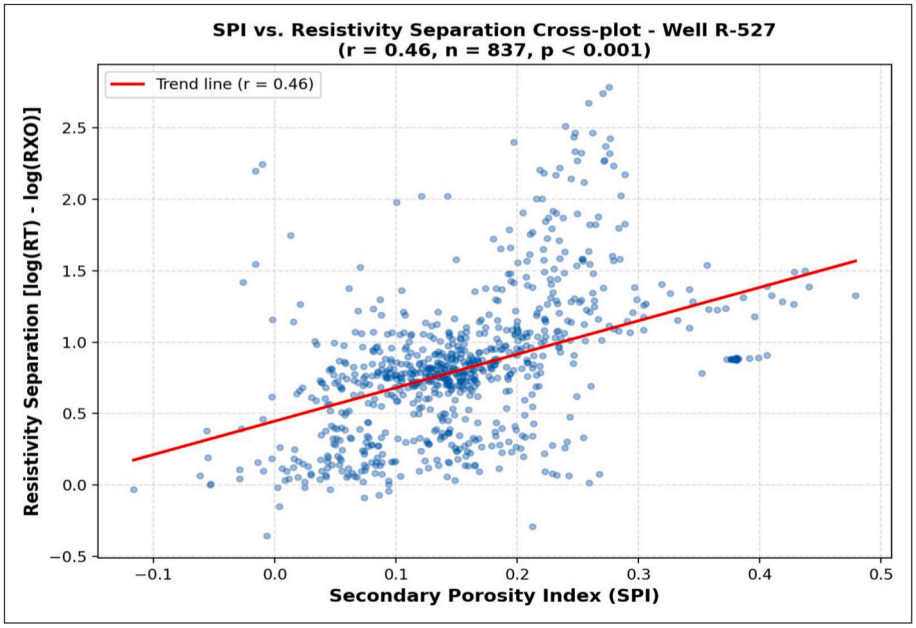


Fig. 22. Cross-plot illustrating the separation between SPI and resistivity for well R-527 (r = 0.46, n = 837, p < 0.001).

conventional well logs. Table 4 and Fig. 20 illustrate the actual behavior of these records in fracture zones observed in the study area.

The secondary porosity index (SPI) was calculated and evaluated to understand the nature of the porous system in the reservoir. High SPI values indicate a significant development in secondary porosity, which is mostly attributed to the presence of natural fracture networks. These fractures play a pivotal role in enhancing secondary porosity and improving the overall performance of the reservoir, with the highest SPI value of 0.75 recorded within the fractured zones. The results of the secondary porosity index (SPI) closely correlate with the resistivity separation analysis in the studied bands. While the SPI registered high values, reaching 0.75, the resistivity curves in the same intervals showed strong positive separation (Fig. 21a–c, e, g). This correlation confirms the presence of a network of open fractures that allowed the penetration of mud filtrate, which not only enhanced the secondary porosity but also significantly improved the reservoir permeability (Fig. 21b–d, f, h).

5.3.2. SPI–resistivity correlation as a fracture diagnostic tool

The connection between resistivity separation and SPI is well-documented in existing studies (Schlumberger, 1991; Asquith et al., 2004; Tiab and Donaldson, 2015). In the same field's carbonate reservoirs, this connection has been used qualitatively, lacking a precise correlation coefficient (Al-Mohsen, 2024). For well R-527, a cross-plot of SPI against resistivity separation was constructed, and a statistically significant positive correlation was observed (r = 0.46, n = 837, p < 0.001) as shown in Fig. 22. This coefficient is moderately linear rather than strongly linear, indicating that SPI and resistivity separation are responding to rock properties that overlap but are not identical. FMI-confirmed fractured intervals in well R-527, such as those at depths of 3130 m and 3158 m, indicate its diagnostic value because both elevated SPI and resistivity separation coincide with open fractures as shown in Fig. 23. This quantitative relationship supports the combined use of SPI and resistivity separation as a diagnostic screening tool for identifying likely fractured intervals in wells lacking image-log data.

6. Discussion

The comprehensive findings of this study indicate that the natural fractures of the Zubair Formation are primarily controlled by tectonic processes, with diagenetic mechanisms playing a minimal role. This results in a highly effective fracture network. Geometric planarity, lateral continuity, and the capacity to cross-cut bedding planes are features of tectonic fractures. These characteristics reflect the consistent regional stress regime under which they formed (Kulander et al., 1990). They originate from the ongoing collision between Arabian and Eurasian plates, particularly since the Miocene, in the Mesopotamian Foredeep Basin (Abdulnaby, 2019). Compared to diagenetic fractures, characterized by their short length, irregularity, and mineral fill, which indicates that they contribute little to present-day fluid flow (Anders et al., 2014). One of the main results is the significant percentage of open fractures (44.25 percent), which is higher than values found in many clastic reservoirs at similar burial depths. This suggests that fracture openness is maintained by either continuous tectonic reactivation or limited late-stage cementation (Laubach et al., 2019; Nelson, 2001). As highly conductive pathways, these open fractures contribute to effective permeability, enabling fluid flow between otherwise isolated porosities of the matrix (Aguilera, 1995); as a result of mineral sealing, closed fractures reduce permeability (Bjørlykke, 2010); while vuggy fractures are less common, they greatly increase storage capacity because of dissolution along fracture planes (Aghli et al., 2020); partially filled fractures represent transitional states with restricted conductivity (Luthi, 2001). Fractures are spatially distributed differently by structural position, with more open fractures observed in crestal wells as compared to flank areas. This is consistent with fold-related fracture models, which predict maximum tensile stress at fold crests (Hennings et al., 2000), thus allowing reservoir development to be targeted at structurally favorable zones in a predictive manner. In addition, the dominant through-going fractures over bedding-confined fractures reveal strong vertical connectivity, which increases interlayer communication and reduces reservoir compartmentation (Cooke and Underwood, 2001; Laubach et al., 2009).

The predominant NW–SE fracture orientation, along with a secondary NE–SW set, is indicative of a conjugate fracture system formed under brittle deformation conditions (Pollard and Fletcher, 2005). The NW-SE fracture pattern previously found for the Mishrif Formation in the same oilfield is consistent with the fracture strike seen in this study (Al-Mohsen and Handhal, 2025). Additionally, this pattern reflects the NW-SE-oriented anticline axis and the regional Zagros fold-thrust trend, both emerging as a result of NE-SW regional compression. On the other hand, the fracture strike does not match the current maximum

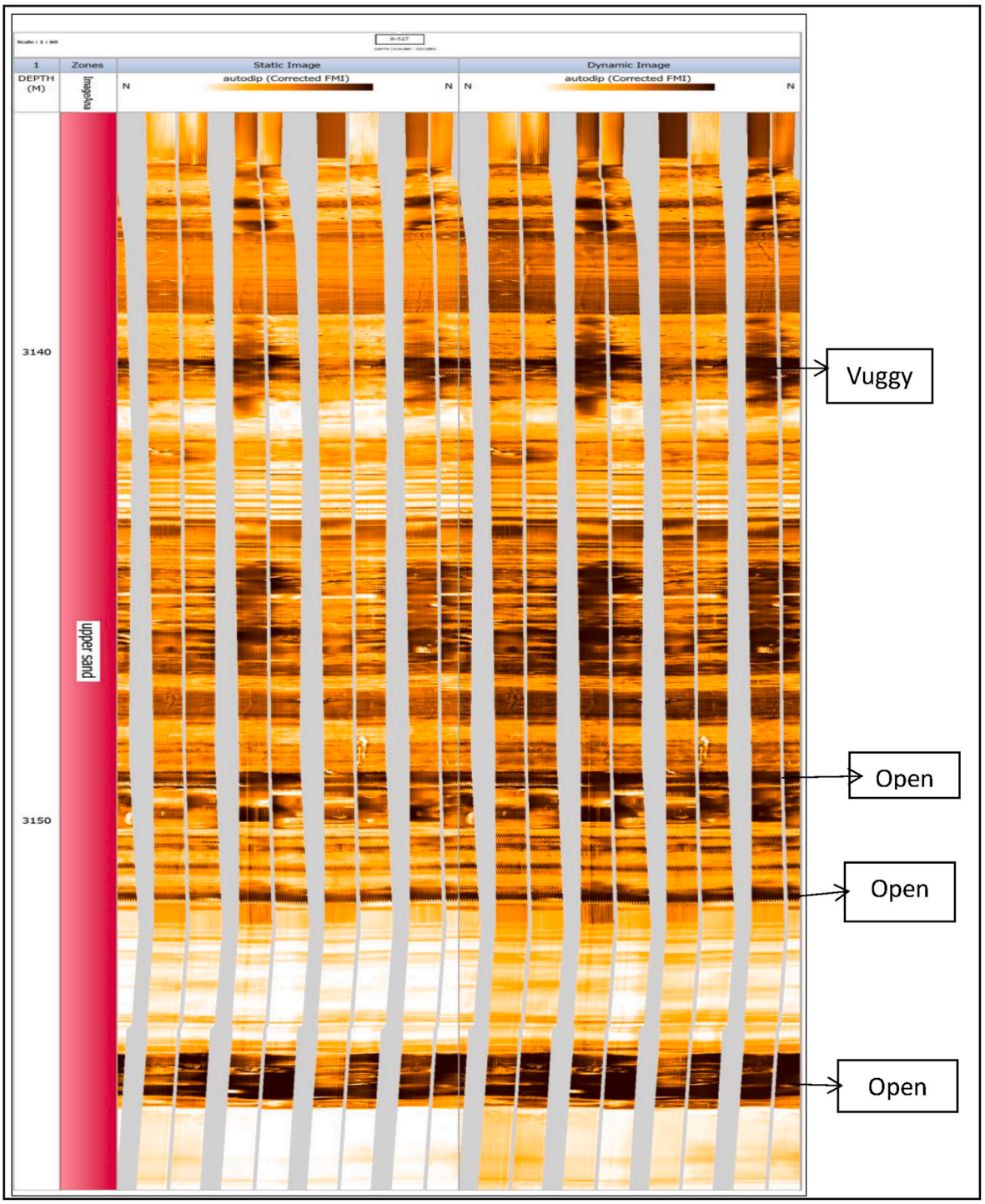


Fig. 23. FMI images, both static and dynamic, for well R-527 (approximately 3134–3157 m) illustrate open and vuggy fractures that align with increased SPI and resistivity separation values.

horizontal stress direction (SHmax), which was determined locally (358°, about N-S) based on a borehole-breakout study in the same oilfield (Jaffar, 2018). Accordingly, the NW-SE fracture set mostly represents fold-related extensional fractures formed during Zagros-related folding, rather than fractures that occurred under current stress. A wide range of calculated fracture permeability (Kf = 52.75–303.84 Darcy) indicates a significant potential for enhanced directional permeability along the NW-SE trend. Supporting these findings, Lazim et al. (2024) analyzed 3D seismic data from the adjacent Zubair oilfield and documented four NW-SE trending folds (Hammar, Shuaila, Rafdya, Safwan) within the Jurassic succession, as well as 47 faults attributed to three tectonic phases: extension, salt activity, and convergence. This systematic pattern produces permeability anisotropy, indicating that horizontal wells should be oriented NE–SW to maximize fracture interception.

Petrophysically, in conventional logs, fractured zones show consistent and diagnostic responses, such as elevated gamma rays because of uranium and thorium enrichment along fracture aperture (Rider, 1986); reduced bulk density as a result of fluid-filled spaces (Schlumberger, 1991); increased sonic transit time and neutron porosity as a result of fluid presence and wave scattering (Asquith et al., 2004; Ellis and Singer,

2007); and a clear sign of open fractures caused by drilling fluid invasion, which are positive separations between deep and shallow resistivity logs (Sibbit and Faivre, 1985). Open fractures contribute significantly to secondary porosity (Tiab and Donaldson, 2015), with Secondary Porosity Index (SPI) values of up to 0.75. In this study, image logs and resistivity data were used to distinguish fracture-related porosity from dissolution-related porosity, even though SPI alone cannot achieve that. This study confirms the dual porosity of the Zubair reservoir, where fractures dominate fluid flow dynamics while the rock matrix provides storage capability (Nelson, 2001).

As a result of the dense network of open fractures, effective permeability is significantly enhanced in units upper shale and upper sand, resulting in a high level of productivity; however, these same fractures may also function as preferential pathways for early water breakthrough during injection processes, potentially reducing sweep efficiency (Cosgrove, 2015) and highlighting the need to incorporate discrete fracture network modeling into reservoir simulation. Large-scale tectonic control has prevailed across the Arabian Plate based on the observed fracture orientations, as well as the proportion of open fractures comparable to that of globally productive fractured reservoirs such as the Troll Field (Wennberg et al., 2016). Although deep burial and diagenetic modification have occurred, the Zubair Formation still has a fracture network that is effective.

This research faced a number of methodological constraints that should be considered when analyzing the findings.

First, only a few wells in the North Rumaila oilfield had well-imaged logs. The diagnosis of fractures in other wells relied on indirect diagnostic techniques, which involved comparing conventional well logs lacking image data with those with actual images (such as electrical resistivity and secondary porosity index). When compared to direct image interpretation, this method created ambiguity.

Second, while this study determined fracture permeability (Kf) by calculating it from fracture width (wf) using a parallel plate flow model based on Poiseuille's equations (Erle, 2015; Tiab and Donaldson, 2015), there were no actual measurements of directional permeability (i.e., permeability measured along the fracture versus across it). Consequently, the relationship between the dominant fracture orientation (NW-SE) and spatial permeability anisotropy is inferred theoretically from the calculated Kf values, rather than confirmed through actual experimental measurements of directional permeability. Additionally, there are intrinsic constraints in the calculation of fracture aperture (wf) using FMI data (Luthi and Souhaite, 1990), which could increase the uncertainty of the Kf values.

Third, instead of being directly derived from well image (FMI) data in this study, the current horizontal maximum stress (SHmax) used for comparing fracture orientation was based on earlier regional research, including fracture measurements from the Rumaila oilfield (Jaffar, 2018). This orientation can differ locally due to the specific location and tectonic history of each well, so caution is needed when extending the relationship between fracture orientation and current stress across the entire field.

Fourth, the study's geographical focus is the North Rumaila Field. The findings and relationships established, such as diagnostic criteria derived from conventional well logs, might need further modification or validation before they can be applied to other geological formations or fields.

Fifth, due to differences in the local lithological composition, structural location, and fracture connectivity, there were differences in the SPI and resistivity separation coefficients between wells. As anticipated, R-527 and R-516 showed acceptable diagnostic correlations ($r = 0.46$ and 0.45, respectively). Other wells examined in this study, however, showed inconsistent or weaker associations. R-527 and R-516 were therefore selected as representative calibration examples, and care should be taken when extrapolating this correlation strength to the full field. The qualitative diagnostic premise of the SPI-resistivity relationship is supported by Asquith and Krygowski (2004), Schlumberger (1991), and Tiab and Donaldson (2015).

Lastly, the fracture density determined in this research is dependent on the number of picks from well images available. It could be influenced by the interpretation software's resolution and sensitivity settings. Therefore, caution is advised when comparing absolute density values across different wells or studies.

7. Conclusion

The following conclusions are obtained from the combined examination of conventional well logs, thin-section petrography, borehole image logs, and core samples from the Zubair Formation: The fracture network in the Zubair Formation, North Rumaila oilfield is a hydraulically conductive and efficient network, where open fractures predominate (44.25%) in addition to the dominance of fractures of tectonic origin in a major direction (NW-SE), which confirms that the distribution of these fractures is not random but rather a regular system governed by the regional stresses of the Zagros Mountains and is primarily responsible for enhancing the porosity and secondary permeability of the reservoir.

In terms of structural control, the majority of open fractures are found in crestal wells (R-516, R-520, and R-491) in units upper shale and upper sand. Fold-related fracture models, in which greatest extension takes place near fold crests, are supported by this distribution pattern.

Fractured intervals have regular and characteristic log responses in petrophysics, such as increased gamma rays, decreased bulk density, increased neutron porosity, increased sonic transit time, positive resistivity separation, and a high value of SPI. These signals offer trustworthy standards for locating fractured zones in wells lacking image log coverage when calibrated using image logs.

This study offers the most thorough multi-scale fracture characterization of the Zubair Formation to date. In addition to supporting optimal oilfield development plans in this and related fields throughout the region, it creates a strong framework for fracture modeling in reservoir simulation.

CRediT authorship contribution statement

Fadia W. Al-Halfi: Data curation, Formal analysis, Methodology, Software, Writing – original draft. **Amna M. Handhal:** Formal analysis, Funding acquisition, Supervision, Writing – review & editing. **Hussein B. Ghalib:** Software, Supervision, Validation.

Declaration of competing interest

The authors declare that they have no known competing financial interests or personal relationships that could have appeared to influence the work reported in this paper.

Data availability

The authors do not have permission to share data.

References

Abdulnaby, W., 2019. Structural geology and neotectonics of Iraq, northwest Zagros. In: Developments in Structural Geology and Tectonics. Elsevier, pp. 53–73. https://doi.org/10.1016/b978-0-12-815048-1.00004-4.

Adams, A.E., MacKenzie, W.S., Guilford, C., 2017. Atlas of Sedimentary Rocks Under the Microscope. Routledge.

Aftab, S., Leisi, A., Kadkhodaie, A., 2023. Reservoir petrophysical index (RPI) as a robust tool for reservoir quality assessment. Earth Sci. Inf. 16, 2457–2473. https://doi.org/10.1007/s12145-023-01049-w.

Aghli, G., Moussavi-Harami, R., Mohammadian, R., 2020. Reservoir heterogeneity and fracture parameter determination using electrical image logs and petrophysical data (a case study, carbonate Asmari Formation, Zagros Basin, SW Iran). Pet. Sci. 17 (1), 51–69. https://doi.org/10.1007/s12182-019-00413-0.

Aguilera, R., 1995. Naturally Fractured Reservoirs, second ed. PennWell Books.

Al-Ameri, T.K., Zumberge, J., 2012. Middle and Upper Jurassic hydrocarbon potential of the Zagross Fold Belt, North Iraq. Mar. Petrol. Geol. 36 (1), 13–34. https://doi.org/10.1016/j.marpetgeo.2012.04.004.
Al-Ansari, R., 1993. The petroleum geology of the Upper Sandstone Member of the Zubair Formation in the Rumaila South [Geological study]. Ministry of Oil, Baghdad, Iraq.
Al-Aradi, H.T., Alnajm, F.M., Al-Khafaji, A.J., 2022. Reservoir properties of the upper sand member of the Zubair Formation in North Rumaila Oil Field. Iraqi Geolog. J. 55 (1C), 97–111. https://doi.org/10.46717/igj.55.1C.8Ms-2022-03-27.
Al-Ismaily, O.S., 2017. Use of Borehole Image Log Technique to Estimate Mishrif Reservoir Characterization in Buzurgan Oilfield [Doctoral dissertation, University of Basrah].
Al-Mohsen, N.A.H.Q., Handhal, A.M., 2025. A comprehensive assessment of natural fractures in the Mishrif Formation: slide studies, core samplings, borehole imaging, and logging techniques. Iraqi J. Sci. https://doi.org/10.24996/ijs.2025.66.4.19.
Al-Mohsen, N.Q., 2024. Characterization of naturally fractured carbonate reservoirs: a case study of Mishrif formation in North Rumaila oilfield. southern Iraq [master's Thesis. University of Basrah, College of Science].
Anders, M.H., Laubach, S.E., Scholz, C.H., 2014. Microfractures: a review. J. Struct. Geol. 69, 377–394. https://doi.org/10.1016/j.jsg.2014.05.011.
Aqrawi, A.A.M., Mahdi, T.A., Sherwani, G.H., Horbury, A.D., 2010. Characterization of the mid-Cretaceous Mishrif reservoir of the southern Mesopotamian basin, Iraq [Paper presentation], 7. American Association of Petroleum Geologists Conference and Exhibition, pp. 7–10.
Asquith, G.B., Krygowski, D., Gibson, C.R., 2004. Basic Well Log Analysis, 16. American Association of Petroleum Geologists, pp. 305–371.
Bjørlykke, K., 2010. Petroleum Geoscience: from Sedimentary Environments to Rock Physics. Springer Science & Business Media.
Buday, T., 1980. The regional geology of Iraq. In: Kassim, S.Z., Jassim, S.Z. (Eds.), Stratigraphy and Paleogeography, 1. Baghdad.
Cooke, M.L., Underwood, C.A., 2001. Fracture Termination and Propagation in Layered Rock. Geological Society, London.
Cosgrove, J.W., 2015. The Association of Folds and Fractures and the Link Between Folding, Fracturing and Fluid Flow During the Evolution of a fold–thrust Belt: a Brief Review. Geological Society, London, Special Publications. https://doi.org/10.1144/SP421.11.
Doll, H.G., 1949. The S.P. log: theoretical analysis and principles of interpretation. Transact. v AIME 179 (1), 146–185. https://doi.org/10.2118/949146-G.
Dong, S., Hao, J., Zeng, L., Yang, X., Wang, L., Ji, C., et al., 2024a. A deep learning object detection method for fracture identification using conventional well logs. IEEE Trans. Geosci. Rem. Sens. 62, 1–16. https://doi.org/10.1109/TGRS.2024.3427364.
Dong, S., Zeng, L., Du, X., Bao, M., Lyu, W., Ji, C., Hao, J., 2022. An intelligent prediction method of fractures in tight carbonate reservoirs. Petrol. Explor. Dev. 49 (6), 1364–1376. https://doi.org/10.1016/S1876-3804(23)60355-6.
Dong, S., Zeng, L., Wang, L., Lyu, W., Xu, H., Ji, C., et al., 2024b. Fracture identification in shale reservoir using a deep learning method: Chang 7 reservoirs, Triassic Yanchang Formation. Geoenergy Sci. Eng. 238, 212853. https://doi.org/10.1016/j.geoen.2024.212853.
Ellis, D.V., Singer, J.M., 2007. Well Logging for Earth Scientists, 692. Springer, pp. 267–288.
Erle, C., 2015. Petrophysics-Theory and Practice of Measuring Reservoir Rock and Fluid Tr. Elsevier Science & Technology, .
Fouad, S.F., 2010. Tectonic and structural evolution of the Mesopotamia Foredeep, Iraq. Iraqi Bull. Geol. Mining 6 (2), 41–53.
Fouad, S.F., Sissakian, V.K., 2011. Tectonic and structural evolution of the Mesopotamia Plain. Iraqi Bull. Geol. Mining 4, 33–46.
Gauthier, B.D.M., Garcia, M., Daniel, J.M., 2002. Integrated fractured reservoir characterization: a case study in a North Africa field. SPE Reserv. Eval. Eng. 5 (04), 284–294. https://doi.org/10.2118/79105-PA.
Handhal, A.M., Ettensohn, F.R., Al-Abadi, A.M., Ismail, M.J., 2022. Spatial assessment of gross vertical reservoir heterogeneity using geostatistics and GIS-based machine-learning classifiers: a case study from the Zubair Formation, Rumaila oil field, southern Iraq. J. Petrol. Sci. Eng. 208 (Part B), 109482. https://doi.org/10.1016/j.petrol.2021.109482.
Handhal, A.M., Jawad, S.M., Al-Abadi, A.M., 2019. GIS-based machine learning models for mapping tar mat zones in upper part (DJ unit) of Zubair Formation in North Rumaila supergiant oil field, southern Iraq. J. Petrol. Sci. Eng. 178, 559–574. https://doi.org/10.1016/j.petrol.2019.03.071.
Hennings, P.H., Olson, J.E., Thompson, L.B., 2000. Combining outcrop data and three-dimensional structural models to characterize fractured reservoirs: an example from Wyoming. AAPG (Am. Assoc. Pet. Geol.) Bull. 84 (6), 830–849.
Jaffar, H.M., 2018. Structural geology of Rumaila Oilfield in southern Iraq from well logs and seismic data. University of Basrah [Unpublished master's thesis].
Jaffar, H.M., 2018. Structural Geology of Rumaila Oilfield in Southern Iraq from Well Logs and Seismic Data. University of Basrah [Unpublished master's thesis].
Jassim, S.Z., Goff, J.C., 2006. Geology of Iraq. DOLIN, S.R.O. distribution with the Geological Society of London.
Kulander, B.R., Dean, S.L., Ward Jr., B.J., 1990. Fractured Core Analysis: Interpretation, Logging, and Use of Natural and Induced Fractures in Core (AAPG Methods in Exploration Series No. 8). American Association of Petroleum Geologists. https://doi.org/10.1306/Mth8516.
Lai, J., Wang, G., Wang, Z., Chen, J., Pang, X., Wang, S., et al., 2018. A review on pore structure characterization in tight sandstones. Earth Sci. Rev. 177, 436–457. https://doi.org/10.1016/j.earscirev.2017.12.003.
Laubach, S.E., Lander, R.H., Criscenti, L.J., Anovitz, L.M., Urai, J.L., Pollyea, R.M., et al., 2019. The role of chemistry in fracture pattern development and opportunities to advance interpretations of geological materials. Rev. Geophys. 57 (4), 1065–1111. https://doi.org/10.1029/2019RG000671.
Laubach, S.E., Olson, J.E., Gross, M.R., 2009. Mechanical and fracture stratigraphy. AAPG (Am. Assoc. Pet. Geol.) Bull. 93 (11), 1413–1426. https://doi.org/10.1306/07270909094.
Lazim, A.A., Handhal, A.M., Rashid, F.N., 2024. Tectonic evolution and structural geology of the Jurassic succession in the Zubair Oil Field, southern Iraq. J. Afr. Earth Sci., 105436 https://doi.org/10.1016/j.jafrearsci.2024.105436.
Leisi, A., Kadkhodaie, A., Kadkhodaie, R., 2026. Integrated reservoir quality index (IRQI): a novel approach for reservoir quality assessment. Sci. Rep. 16, 10596. https://doi.org/10.1038/s41598-026-46154-0.
Leisi, A., Khojasteh, E.R., Manaman, N.S., 2025. Integrated neural network–geostatistical modeling for data-driven estimation of shear wave velocity from conventional well logs: a case study from an Iranian oil reservoir. Results Eng., 108855 https://doi.org/10.1016/j.rineng.2025.108855.
Leisi, A., Shad Manaman, N., 2025a. Geomechanical characterization of Asmari Formation in the Dezful embayment via simultaneous inversion and extended elastic impedance techniques, SW Iran. Earth Sci. Inf. 18, 337. https://doi.org/10.1007/s12145-025-01853-6.
Leisi, A., Shad Manaman, N., 2025b. Seismic and geomechanical characterization of Asmari formation using well logs and simultaneous inversion in an Iranian oil field. Sci. Rep. 15, 11276. https://doi.org/10.1038/s41598-025-95796-z.
Lorenz, J.C., Cooper, S.P., 2017. Atlas of Natural and Induced Fractures in Core. John Wiley & Sons.
Luthi, S.M., 2001. Geological Applications of Well Logs: Methods in Geomathematics. Springer-Verlag Berlin Heidelberg.
Luthi, S.M., Souhaite, P., 1990. Fracture apertures from electrical borehole scans. Geophysics 55 (7), 821–833.
Mohammed, W.J., Al-Jawad, M.S., Al-Shamma, D.A., 2010. Reservoir flow simulation study for a sector in Main Pay-South Rumaila Oil Field. In: [Paper presentation]. SPE Oil and Gas India Conference and Exhibition. https://doi.org/10.2118/126427-MS.
Narr, W., Schechter, D.S., Thompson, L.B., 2006. Naturally Fractured Reservoir Characterization. Society of Petroleum Engineers. https://doi.org/10.2118/9781613999615.
Nelson, R., 2001. Geologic Analysis of Naturally Fractured Reservoirs, second ed. Gulf Professional Publishing.
Owen, R.M.S., Nasr, S.N., 1958. Stratigraphy of the Kuwait-Basra Area. Middle East.
Pollard, D.D., Fletcher, R.C., 2005. Fundamentals of Structural Geology. Cambridge University Press.
Rider, M., 1986. The Geological Interpretation of Well Logs. Blackie & Son.
Saleh, A.H., 2019. Depositional environment and diagenesis processes impact on the carbonate rock quality: a case study, southeastern of Iraq. Iraqi J. Sci. 60 (5), 1104–1114. https://doi.org/10.24996/ijs.2019.60.5.19.
Schlumberger Limited, 1991. Log Interpretation principles/applications. Schlumberger Educational Services.
Shafiei, A., Dusseault, M.B., Kosari, E., Taleghani, M.N., 2018. Natural fractures characterization and in situ stresses inference in a carbonate reservoir—An integrated approach. Energies 11 (2). https://doi.org/10.3390/en11020312, 312.
Shehab, M.N., Al-Najm, F.M., Al-Kaabi, M.H., 2023. Image log facies and lost circulation of the Dammam Formation in Rumaila Oil Field, southern Iraq. Iraqi Geolog. J. 56 (1C), 150–168. https://doi.org/10.46717/igj.56.1C.10ms-2023-3-21.
Sibbit, A.M., Faivre, O., 1985. The dual laterolog response in fractured rocks. In: [Paper presentation]. SPWLA 26th Annual Logging Symposium, Society of Petrophysicists and Well Log Analysts.
Tiab, D., Donaldson, E.C., 2015. Petrophysics: Theory and Practice of Measuring Reservoir Rock and Fluid Transport Properties, fourth ed. Gulf Professional Publishing. https://doi.org/10.1016/C20140037070.
Wells, M., Morton, A., Frei, D., 2017. Provenance of Lower Cretaceous clastic reservoirs in the Middle East. J. Geol. Soc. 174, 1048–1061. https://doi.org/10.1144/jgs2017-013.
Wennberg, O.P., Casini, G., Jonoud, S., Peacock, D.C., 2016. The characteristics of open fractures in carbonate reservoirs and their impact on fluid flow: a discussion. Pet. Geosci. 22 (1), 91–104. https://doi.org/10.1144/petgeo2015-003.
Zhao, Y., Ren, Z., Chen, X., He, W., Zhang, Z., Wei, Z., Hu, Y., 2025. Fracture prediction based on a complex lithology fracture facies model: a case study from the Linxing area, Ordos Basin. Appl. Sci. 15 (24), 13277. https://doi.org/10.3390/app152413277.